2014

MODELING AND VALIDATION OF A SYNCHRONOUS-MACHINE/ CONTROLLED-RECTIFIER SYSTEM

Kyle A. Hord
University of Kentucky, kahord@gmail.com

STUDENT AGREEMENT:

I represent that my thesis or dissertation and abstract are my original work. Proper attribution has been given to all outside sources. I understand that I am solely responsible for obtaining any needed copyright permissions. I have obtained needed written permission statement(s) from the owner(s) of each third-party copyrighted matter to be included in my work, allowing electronic distribution (if such use is not permitted by the fair use doctrine) which will be submitted to UKnowledge as Additional File.

I hereby grant to The University of Kentucky and its agents the irrevocable, non-exclusive, and royalty-free license to archive and make accessible my work in whole or in part in all forms of media, now or hereafter known. I agree that the document mentioned above may be made available immediately for worldwide access unless an embargo applies.

I retain all other ownership rights to the copyright of my work. I also retain the right to use in future works (such as articles or books) all or part of my work. I understand that I am free to register the copyright to my work.

REVIEW, APPROVAL AND ACCEPTANCE

The document mentioned above has been reviewed and accepted by the student's advisor, on behalf of the advisory committee, and by the Director of Graduate Studies (DGS), on behalf of the program; we verify that this is the final, approved version of the student's thesis including all changes required by the advisory committee. The undersigned agree to abide by the statements above.

Kyle A. Hord, Student

Dr. Aaron Cramer, Major Professor

Dr. Cai-Cheng Lu, Director of Graduate Studies

MODELING AND VALIDATION OF A SYNCHRONOUS-MACHINE/CONTROLLED-RECTIFIER SYSTEM

THESIS

A thesis submitted in partial fulfillment of the
requirements for the degree of Master of Science in Electrical Engineering in the
College of Engineering
at the University of Kentucky

By

Kyle Hord

Lexington, Kentucky

Director: Dr. Aaron M. Cramer, Assistant Professor, Electrical Engineering

Lexington, Kentucky

2014

ABSTRACT OF THESIS

MODELING AND VALIDATION OF A SYNCHRONOUS-MACHINE/CONTROLLED-RECTIFIER SYSTEM

The hardware validation of a novel average-value model (AVM) for the simulation of a synchronous-generator/controlled rectifier system is presented herein. The generator is characterized using genetic algorithm techniques to fit standstill frequency response (SSFR) measurements to *q* and d-axis equivalent circuits representing the generator in the rotor reference frame. The generator parameters form the basis of a detailed model of the system, from which algebraic functions defining the parametric AVM are derived. The average-value model is compared to the physical system for a variety of loading and operating conditions including step load change, change in delay angle, and external closed-loop control, validating the model accuracy for steady-state and transient operation.

KEYWORDS: Average-value model, synchronous machine, three-phase controlled rectifier, hardware validation, standstill frequency response (SSFR)

Kyle Hord

5/1/2014

MODELING AND VALIDATION OF A SYNCHRONOUS-MACHINE/CONTROLLED-RECTIFIER SYSTEM

By

Kyle Hord

Dr. Aaron Cramer
Director of Thesis

Dr. Cai-Cheng Lu
Director of Graduate Studies

5/1/2014
Date

ACKNOWLEDGEMENTS

This work could not have been completed without the support, expertise, and guidance provided by numerous professors, staff, and students. The author would like to personally thank the following people for their contributions: Dr. Aaron Cramer, Dr. Yuan Liao, Dr. Joseph Sottile, Richard Anderson, Fei Pan, Hanling Chen, Xiao Liu, Mengmei Liu, Jing Shang, Wei Zhu, and Ying Li.

TABLE OF CONTENTS

LIST OF TABLES

LIST OF FIGURES

1. INTRODUCTION

Synchronous machines, specifically synchronous generators, are extremely important components in power generation systems worldwide. The primary means by which mechanical energy is converted to electrical energy for distribution and consumption is by synchronous generators. In applications where large direct-current power is needed, such as high-power DC supplies, excitation of large generators [1], aircraft power systems [2], and shipboard and submarine power systems, synchronous-generator/controlled-rectifier systems are commonly used.

Control of these systems can be executed by regulation of the machine excitation voltage. By controlling the excitation at the field winding of the machine, the DC output voltage of the system is maintained. Unfortunately this method of control can be slow and is not useful if rapid regulation of the DC output voltage is necessary. In such cases it is beneficial to employ a controlled rectifier and regulate the system via control of the converter.

As a tool for development and design, computer simulation of the switching dynamics of the synchronous-generator/controlled-rectifier system is very powerful. Unfortunately, while detailed models of such systems exist, based on the modeling of the switching behavior of each diode in the rectifier, they can lack practical value for system simulation due to their intensive computational demands [3].

In order to work around this limitation of the detailed model, researchers have developed the application of Average-Value Models, or AVMs, to the simulation of controlled-rectifier systems. AVMs simplify the demands of simulation and neglect the effects of fast switching by averaging with respect to the switching interval. The result is a simulation method that can predict the salient aspects of system behavior with fewer computational resources and in less time. This allows researchers to study a different variety and complexity of system behavior, to predict

system dynamics over a longer time span, and to use such simulation as a suitable tool for control and system-level studies.

This study examines the application of a novel AVM technique to a particular physical synchronous-generator/controlled-rectifier system. The aim of the research is to validate experimentally the accuracy of the AVM simulation for hardware.

2. BACKGROUND REVIEW

Synchronous Generators

A synchronous generator is an electrical machine used to convert mechanical energy to electrical energy. The key operating principle of a synchronous generator is magnetic induction as described in Faraday's Law, stating that a changing (or rotating) magnetic field will induce current to flow in a nearby conductor.

The main components of a generator are the stator (stationary) and the rotor (rotating). The rotor, which contains an electromagnet or field winding, produces the main magnetic field of the machine, which rotates within the stator and induces current in the stator windings. The stator is a stationary cylindrical member containing the stator or armature windings and encasing the rotor. Stator windings correspond to the three output phases of the machine and are embedded in the inner stator wall in slots. For a three-phase machine, the stator consists of three identical windings. They are assumed to be sinusoidally distributed around the stator circumference, with each phase separated by 120°. This arrangement ensures that the induced voltages on the phase outputs produce a balanced, three-phase set.

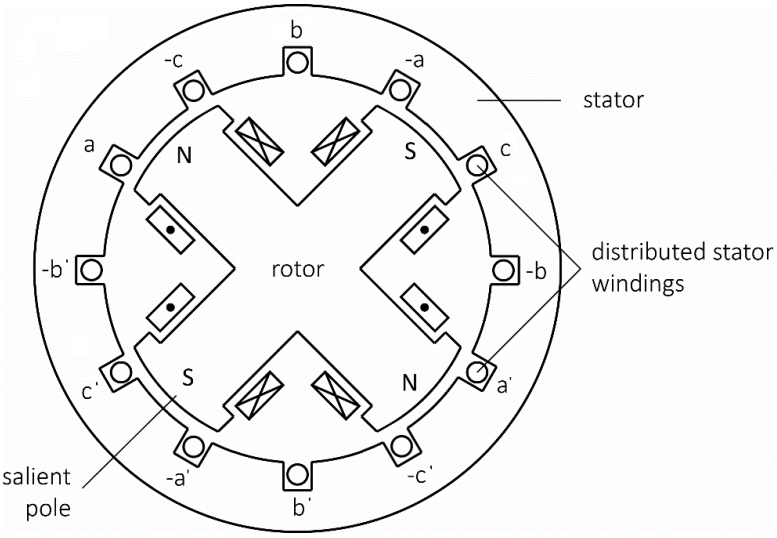

Figure 1. Four-pole, Three-Phase Salient Pole Synchronous Generator

The rotor consists of electromagnetic coils which are energized by a voltage to generate the main magnetic field of the machine as well as damper windings. The synchronous machine studied herein is a four-pole salient-rotor design, meaning there are four windings corresponding to the opposing poles of two electromagnets, evenly spaced around the rotor circumference. Such a design consists of a rotor shape resembling a cross, in which each pole is wrapped on a core extending from the center. The ends of the poles have curved "shoes" which allow for a suitable air gap at the poles. Damper windings are shorted windings in the rotor which serve to improve the response and stability of the machine by creating induced currents which aid machine synchronization. When the machine operates at steady state, the damper windings have no induced current.

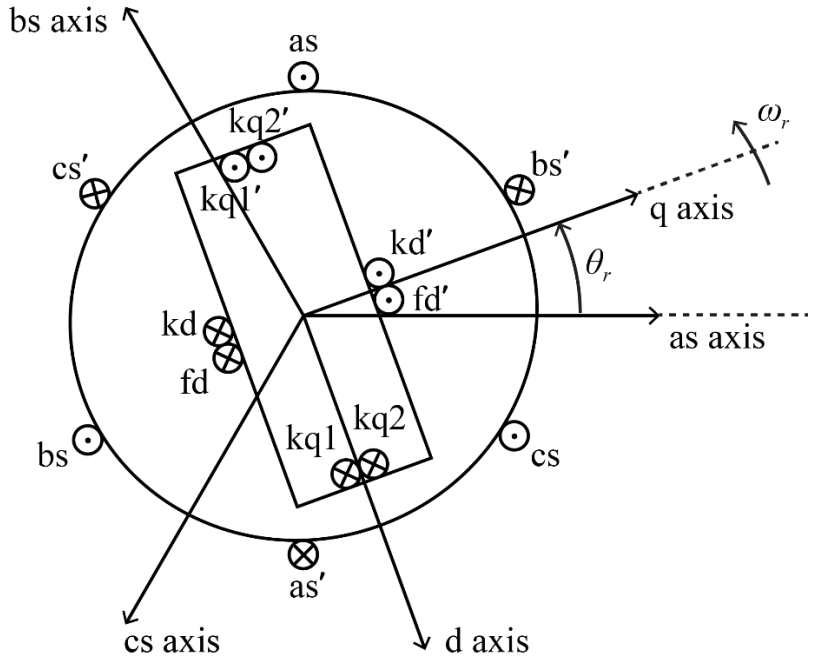

Figure 2. Two-Pole Synchronous Generator Windings and Construction

In many synchronous machines, the excitation voltage for the field windings comes from a second smaller generator with armature windings on the larger rotor. When the main generator spins, an AC voltage is induced in the armature of the exciter, and this voltage is converted by a

rotating rectifier to supply the DC voltage necessary for field excitation. This design is known as a brushless exciter.

The basis for mathematically describing a synchronous machine can be developed by analysis of a representative machine. A two-pole, three-phase, wye-connected, salient-pole synchronous machine is show in **Figure 2**. The stator windings *as, bs,* and *cs* are identical, sinusoidally-distributed windings with N_s equivalent turns and resistance r_s. The rotor consists of one field winding with N_{fd} equivalent turns and resistance r_{fd} and three damper windings. The *kd* damper winding has the same magnetic axis as the *fd* winding with N_{kd} equivalent turns and resistance r_{kd} while the *kq1* and *kq2* (*q*-axis) damper windings are perpendicular to the *fd* and *kd* (*d*-axis) windings and have equivalent turns N_{kq1} and N_{kq2} and resistances r_{kq1} and r_{kq2}, respectively.

The voltage equations of the synchronous machine can be expressed in matrix form as:

$$\mathbf{v}_{\boldsymbol{abcs}} = \mathbf{r}_{\boldsymbol{s}}\mathbf{i}_{\boldsymbol{abcs}} + p\boldsymbol{\lambda}_{\boldsymbol{abcs}} \tag{1}$$

$$\mathbf{v}_{\boldsymbol{qdr}} = \mathbf{r}_{\boldsymbol{r}}\mathbf{i}_{\boldsymbol{qdr}} + p\boldsymbol{\lambda}_{\boldsymbol{qdr}} \tag{2}$$

where

$$(\mathbf{f}_{\boldsymbol{abcs}})^T = [f_{as} \quad f_{bs} \quad f_{cs}] \tag{3}$$

$$\left(\mathbf{f}_{\boldsymbol{qdr}}\right)^T = [f_{kq1} \quad f_{kq2} \quad f_{fd} \quad f_{kd}] \tag{4}$$

and *s* and *r* subscripts refer to variables associated with the stator and rotor, respectively. The resistance matrices $\mathbf{r}_{\boldsymbol{s}}$ and $\mathbf{r}_{\boldsymbol{r}}$ are defined as follows:

$$\mathbf{r}_{\boldsymbol{s}} = \mathrm{diag}[r_s \quad r_s \quad r_s] \tag{5}$$

$$\mathbf{r}_{\boldsymbol{r}} = \mathrm{diag}[r_{kq1} \quad r_{kq2} \quad r_{fd} \quad r_{kd}] \tag{6}$$

Given these variables, the flux linkage equations may be expressed as

$$\begin{bmatrix} \boldsymbol{\lambda}_{abcs} \\ \boldsymbol{\lambda}_{qdr} \end{bmatrix} = \begin{bmatrix} \mathbf{L}_s & \mathbf{L}_{sr} \\ (\boldsymbol{L}_{sr})^T & \mathbf{L}_r \end{bmatrix} \begin{bmatrix} \mathbf{i}_{abcs} \\ \mathbf{i}_{qdr} \end{bmatrix} \tag{7}$$

The inductance matrices above can be expanded in terms of standard machine inductances as seen in Section 5.2 of [4]. When expanded, the stator-related inductance matrices $\mathbf{L}_{sr}$ and $\mathbf{L}_r$ are seen to be dependent upon the rotor angular displacement, θ_r. If the rotor spins, the rotor position varies with time, meaning that these inductances are time-varying. In order to alleviate this complexity, a technique called reference frame theory is used to transform the machine equation variables.

Reference Frame Theory

Due to the inherent complexity of the basic equations derived to describe the variables and inductances of a rotating electric machine, specifically a synchronous machine, and the numerous time-varying quantities introduced in these derivations, new formulations or transformations of the equations have been developed in order to simplify them. Similar to a change of variables such as a transformation from rectangular to polar coordinates, a reference frame transformation provides a different but equally valid representation of synchronous machine equations, ideally one that facilitates solving or calculation. The most general and most useful of such transformations consists of a transformation or change of variables from the stator components of a synchronous machine to components of virtual windings rotating within the rotor.

This transformation, known as the rotor reference frame, eliminates all time-varying inductances from the voltage equations of the machine. The former stator quantities are transformed into virtual rotating windings in the rotor. Since both stator and rotor windings now rotate, there is no dependence upon the rotor angular displacement, θ_r, in the machine inductances. Rotor reference frame theory, as developed in the 1920's by R.H. Park [5],

completely changed electric machine analysis. In the following years, other researchers developed new variations of reference frame theory. Park's transformation is in fact a specific case of a general transformation that refers machine variables to a reference frame rotating at an arbitrary angular velocity [5]. The general transformation is performed with the following equations:

$$\boldsymbol{f}_{qd0s} = \boldsymbol{K}_s \boldsymbol{f}_{abcs} \tag{8}$$

$$\boldsymbol{K}_s = \frac{2}{3}\begin{bmatrix} \cos(\theta) & \cos\left(\theta - \frac{2\pi}{3}\right) & \cos\left(\theta + \frac{2\pi}{3}\right) \\ \sin(\theta) & \sin\left(\theta - \frac{2\pi}{3}\right) & \sin\left(\theta + \frac{2\pi}{3}\right) \\ 1/2 & 1/2 & 1/2 \end{bmatrix} \tag{9}$$

$$\left(\boldsymbol{f}_{qd0s}\right)^T = [f_{qs} \quad f_{ds} \quad f_{0s}] \tag{10}$$

$$(\boldsymbol{f}_{abcs})^T = [f_{as} \quad f_{bs} \quad f_{cs}] \tag{11}$$

$$\omega = \frac{d\theta}{dt} \tag{12}$$

In this general transformation, $\boldsymbol{f}$ can stand for voltage, current, flux linkage, or electric charge. The angular position θ must be continuously differentiable, but otherwise has no specified value, and can therefore be any time-varying or fixed value, including zero. There is no real physical form for the transformed variables with *q*, *d*, and 0 subscripts, but these variables and their interrelation can be visualized in a helpful manner in **Figure 3**. As a balanced set, f_{as}, f_{bs}, and f_{cs}, can be represented as stationary variables evenly spaced by 120°. The variables represented by f_{qs} and f_{ds} are then represented as an orthogonal set rotating at an angular velocity of ω. The *a*, *b*, and *c* variables can also be interpreted as the direction of the magnetic axes of the stator windings while the transformed *q* and *d* components can interpreted as the transformed or rotor-refered magnetic axes.

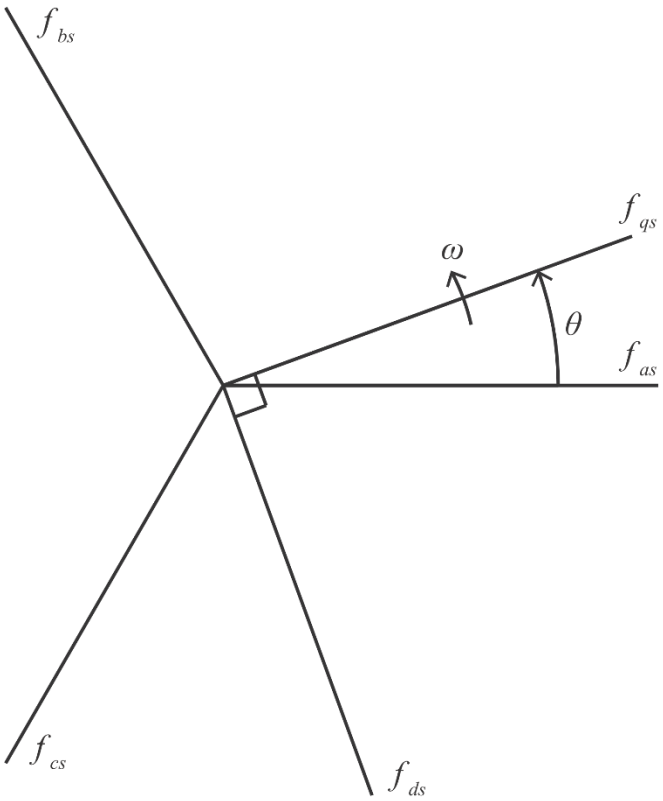

Figure 3. General Reference Frame Respresentation

It is also helpful to refer rotor quantities to the stator of an electric machine before the reference frame transformation is performed. This is similar to referring quantities from one winding of a transformer to another and is accomplished with the following equations, where *j* is a placeholder for rotor quantity subscripts *fd*, *kd*, *kq1*, or *kq2*:

$$i'_j = \frac{2}{3}\frac{N_j}{N_s} i_j \tag{13}$$

$$v'_j = \frac{N_s}{N_j} v_j \tag{14}$$

$$\lambda'_j = \frac{N_s}{N_j} \lambda_j \tag{15}$$

Single-Phase Rectifier

A basic discussion of rectification is provided here as background for the discussion of the three-phase controlled rectifier as studied herein. For a more detailed analysis, refer to [6].

The uncontrolled single phase rectifier is a fundamental power electronics device employed to convert an AC input voltage to a DC output voltage. This is accomplished by the use of diodes to selectively restrict and allow the flow of current such that the load current only flows in one direction and the load voltage polarity does not change.

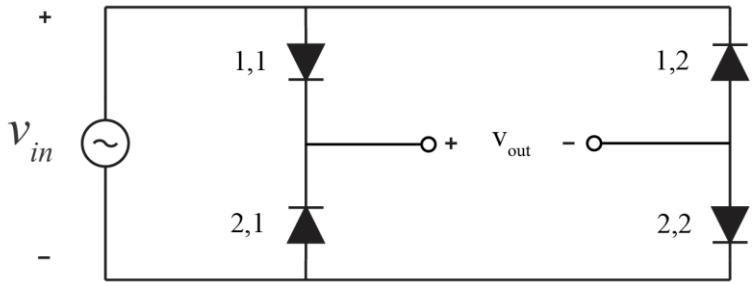

Figure 4. Single Phase Full Bridge Rectifier

A basic full-bridge rectifier is seen in **Figure 4**. During the positive half-cycle, or when the sinusoidal source voltage and current are positive (with respect to the source polarity as labeled), current flows from the positive terminal of the source, through D_{11}, into the positive terminal of the load, through D_{22}, and back to the negative terminal of the source. During the negative half-cycle, current flows from the negative terminal of the source, through D_{21}, into the positive terminal of the load, through D_{12}, and back to the positive terminal of the source. Current flowing from the positive source terminal is blocked by D_{12}. Likewise, current flowing from the negative source terminal is blocked by D_{22}. Current can only flow into the positive terminal of the load, ensuring that load current and voltage are DC and maintain consistent polarity.

The DC voltage at the load is calculated as the average value of the resultant waveform (see **Figure 5**, $\alpha = 0$). If the input voltage is assumed to be:

$$v_{in} = \sqrt{2}E\cos\omega t \tag{16}$$

where E is the rms voltage, then the output voltage can be expressed as follows:

$$v_{out} = \begin{cases} \sqrt{2}E\cos\omega t\,, & -\frac{\pi}{2} \le \omega t \le \frac{\pi}{2} \\ -\sqrt{2}E\cos\omega t\,, & \frac{\pi}{2} \le \omega t \le \frac{3\pi}{2} \end{cases} \tag{17}$$

During the half-cycle when the source voltage is positive, the output voltage is equal to the input. During the negative half-cycle, the output voltage is equal to the negative of the input. Thus, the load voltage will always be positive.

The average voltage of the load can then be calculated by integrating the output voltage over one period:

$$\bar{v}_{out} = \int_{-\frac{\pi}{2}}^{\frac{\pi}{2}} \sqrt{2}E\cos\omega t\, dt = \frac{2\sqrt{2}}{\pi}E \tag{18}$$

Single-Phase Controlled Rectifier

If control of the output voltage level is required, a controlled rectifier can be implemented by replacing diodes with thyristors. Thyristors, also known as silicon-controlled rectifiers (SCRs), are similar to diodes but have a gating signal which controls forward conduction in the device. Current can only flow when the device is both forward biased and a firing pulse is applied to the gate. The device will stop conducting when it becomes reverse biased. Control of the output voltage level is provided by changing the timing of the firing pulse relative to the moment when a diode is forward biased. This delay angle, α, is known as the firing angle.

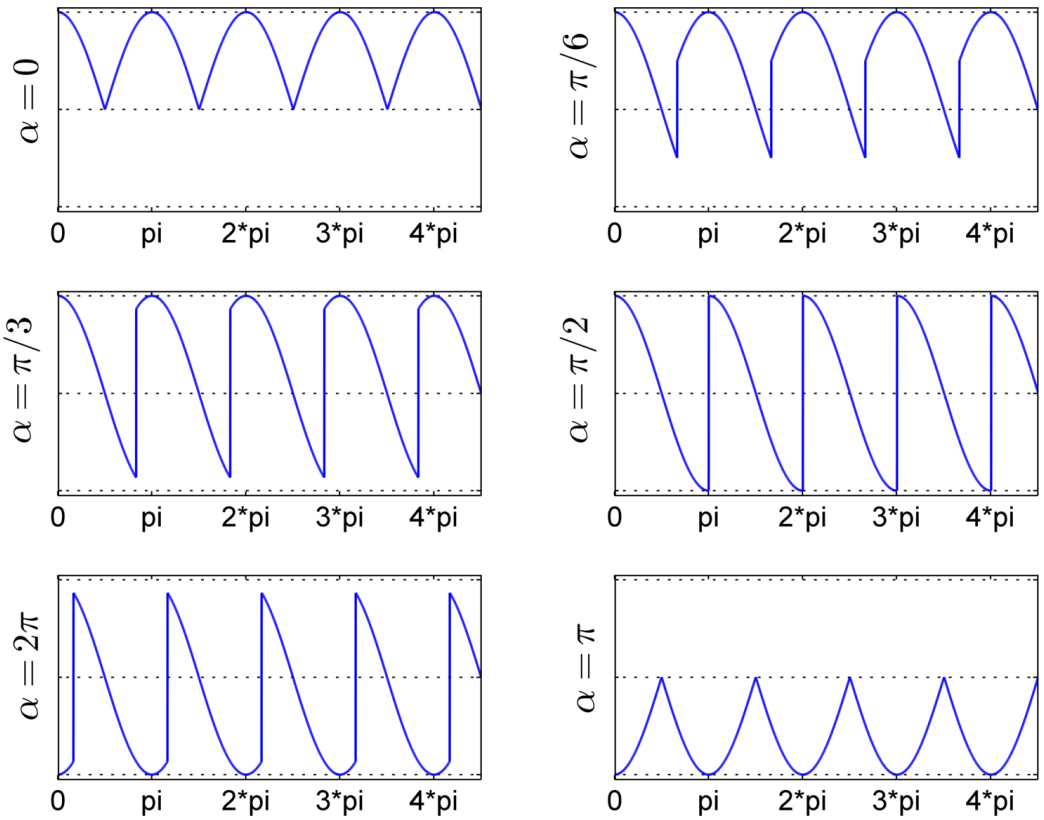

Figure 5. Output voltage waveforms for controlled rectifier, shown as $v_{out}/\sqrt{2}$ E vs. $\omega t/\pi$

Sample waveforms of the controlled rectifier can be seen in **Figure 5**. For $\alpha = 0$, the controlled-rectifier operates identically to the uncontrolled rectifier, since there is no delay between forward biasing and firing. The output voltage corresponds to the periodic repetition of a half-cycle of the input. For zero delay this repeated interval comprises the entire positive half-cycle. Graphically one can imagine the interval delaying as α increases, the output voltage now consisting of intervals of both positive and negative half-cycles. At $\alpha = \pi/2$, the output consists of equal intervals of positive and negative half-cycles, thus indicating an average voltage of zero. For $\alpha > \pi/2$, the average output voltage becomes negative, until reaching $\alpha = \pi$, where the output voltage consists of the periodic repetition of the entire negative half-cycle. The average output voltage is proportional to $\cos\alpha$, decreasing from a maximum at $\alpha = 0$, reaching zero at

$\alpha = \pi/2$, and reaching a minimum at $\alpha = \pi$. For a resistive load, delay angles greater than $\alpha = \pi/2$ are not relevant. The average output voltage is calculated as follows:

$$\bar{v}_{out} = \int_{-\frac{\pi}{2}+\alpha}^{\frac{\pi}{2}+\alpha} \sqrt{2}E \cos \omega t \, dt = \frac{2\sqrt{2}}{\pi} E \cos \alpha \tag{19}$$

An important additional effect to consider is that of a non-zero AC-side inductance, or commutating inductance L_C (see **Figure 6**). Commutating inductance causes the switching of thyristors to be non-instantaneous. In an ideal converter, only two switches (T1 and T3, or T2 and T4) are closed at a time. Commutating inductance leads to modes in which more than two switches are closed, effectively short-circuiting the output current and nulling the output voltage. This has the effect of reducing the average output voltage:

$$\bar{v}_{out} = \frac{2\sqrt{2}}{\pi} E \cos \alpha - \frac{\omega_e L_c}{\pi} I_d \tag{20}$$

Three-Phase Controlled Rectifier

The three-phase controlled rectifier used in this study is typically known as a three-phase fully-controlled bridge rectifier. **Figure 6** shows this topology.

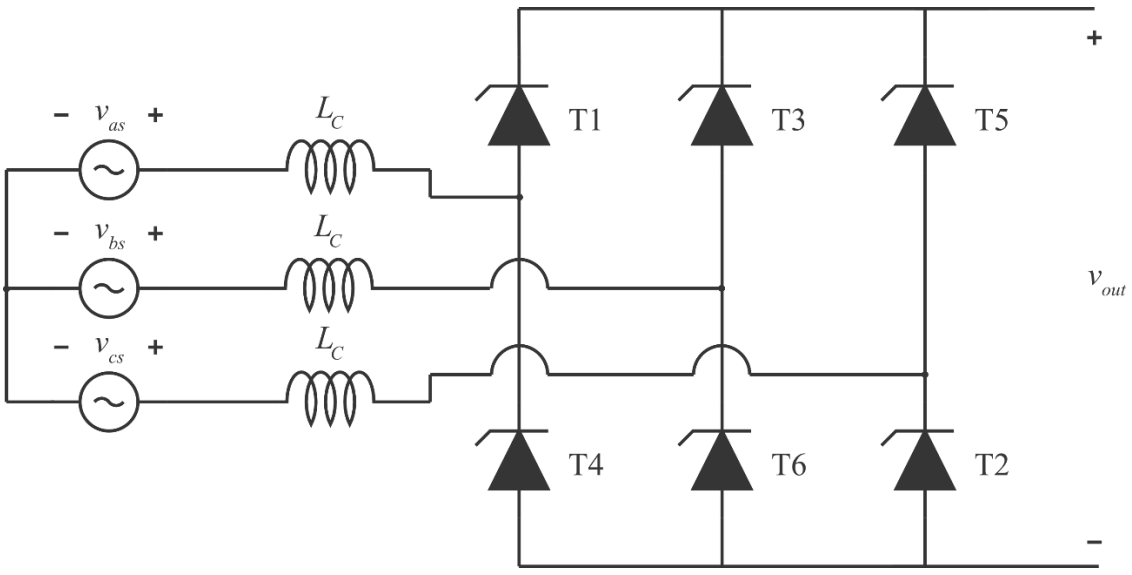

Figure 6. Three-Phase Controlled Full-Bridge Rectifier

The voltage sources are line-to-neutral, with v_{as} as the reference, v_{as} leading v_{bs} by 120°, and v_{bs} leading v_{cs} by 120°. The source voltages can be defined as follows:

$$v_{as} = \sqrt{2}E\cos\omega t \tag{21}$$

$$v_{bs} = \sqrt{2}E\cos\left(\omega t - \frac{2\pi}{3}\right) \tag{22}$$

$$v_{cs} = \sqrt{2}E\cos\left(\omega t + \frac{2\pi}{3}\right) \tag{23}$$

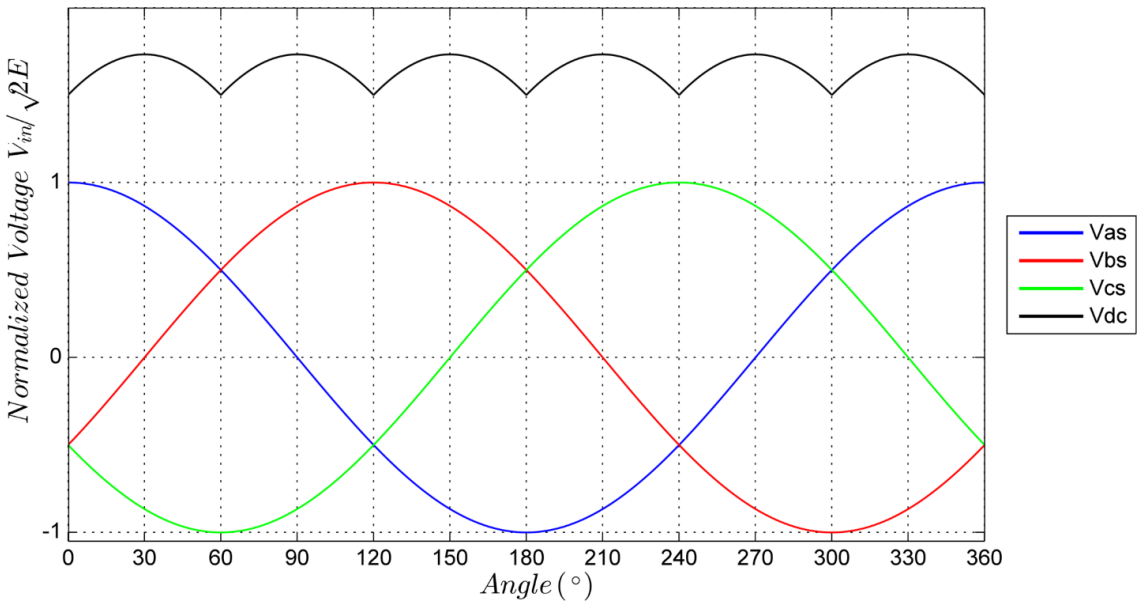

Figure 7. Source and Output Voltage Waveforms for 3-Ø Controlled Rectifier, α=0

The SCRs are switched such that different intervals of input voltage will be present on the output. Each SCR fires for one third of the period, with SCRs overlapping to create six distinct intervals. These intervals are apparent in the nodes of the DC output voltage for $\alpha = 0$ as seen in **Figure 7**. Each interval or node represents a different line-to-line voltage and switch combination. For example, the first node occurs when T1 and T2 are on. This combination connects v_{as} to the positive load terminal and v_{cs} to the negative load terminal. The voltage at the load is then v_{as} - v_{cs}, or V_{ac}, a line-to-line voltage.

$$V_{ab} = v_{as} - v_{bs} = \sqrt{6}E\cos\left(\omega t - \frac{\pi}{6}\right) \tag{24}$$

Accordingly, the output voltage intervals can be fully described as follows:

Table 1. Voltage Intervals for Output of 3-Ø Controlled Rectifier

Interval/Angle			SCR Firing	Output Voltage
$\boldsymbol{\alpha}$	to	$\frac{\pi}{3}+\alpha$	T1 and T2	$v_{as}-v_{cs}=V_{ac}$
$\frac{\boldsymbol{\pi}}{\boldsymbol{3}}+\boldsymbol{\alpha}$	to	$\frac{2\pi}{3}+\alpha$	T2 and T3	$v_{bs}-v_{cs}=V_{bc}$
$\frac{\boldsymbol{2\pi}}{\boldsymbol{3}}+\boldsymbol{\alpha}$	to	$\pi+\alpha$	T3 and T4	$v_{bs}-v_{as}=V_{ba}$
$\boldsymbol{\pi}+\boldsymbol{\alpha}$	to	$\frac{4\pi}{3}+\alpha$	T4 and T5	$v_{cs}-v_{as}=V_{ca}$
$\frac{\boldsymbol{4\pi}}{\boldsymbol{3}}+\boldsymbol{\alpha}$	to	$\frac{5\pi}{3}+\alpha$	T5 and T6	$v_{cs}-v_{bs}=V_{cb}$
$\frac{\boldsymbol{5\pi}}{\boldsymbol{3}}+\boldsymbol{\alpha}$	to	α	T6 and T1	$v_{as}-v_{bs}=V_{ab}$

The average output voltage can be calculated by integrating over any one of these intervals:

$$\bar{v}_{out}=\frac{3}{\pi}\int_{\alpha}^{\frac{\pi}{3}+\alpha}\sqrt{6}E\cos\left(\omega t-\frac{\pi}{6}\right)dt=\frac{3\sqrt{6}}{\pi}E\cos\alpha \tag{25}$$

As α increases, the portion of the input waveforms that is present at the output shifts, decreasing the average DC voltage as the line-to-line voltages decrease. The full range of alpha is $0\leq\alpha<\pi$; however, if the load cannot supply average power, only angles from $0\leq\alpha\leq\frac{\pi}{2}$ are relevant.

Additionally, if the converter is connected to a dc load with a non-constant current, the equations above can only approximate converter outputs. For these conditions a computer simulation such as an average value model is more useful and practical.

For analysis, it is convenient to classify the operation of the rectifier by modes based on the states of conduction during a line period. Mode 0 is designated when no diodes are conducting during a line period [7]. Mode 1 contains intervals of non-conduction and intervals in which two

diodes are conducting within the same line period. Mode 2 consists of intervals of non-conduction, two diodes conducting, and three diodes conducting. Mode 3 contains intervals of two diodes conducting and intervals of three diodes conducting, but no intervals of non-conduction. Mode 4 consists of only intervals in which three diodes are conducting, corresponding to the continuous current mode of operation [7].

Average Value Modeling

Average Value Modeling is a unique and beneficial approach to the issue of system stability studies of power electronics. Owing to the widespread usage of synchronous-machine/controlled-rectifier systems in aircraft and ship power systems, excitation of larger generators, wind power generation, and other sources and loads relying on power electronics, the stability of such systems is a critical issue [3]. The development of Average Value Models (AVMs) has been necessitated by the computationally intensive nature of traditional modeling for such systems, in which the detailed behavior of each switch is modeled individually. These models provide accurate simulation of such systems but are computationally intensive in general and therefore not suitable for many studies.

An AVM approach circumvents this problem by neglecting or “averaging” the effects of the fast switching with respect to the switching interval. In this sense it approximates the salient long-term dynamics of a system without the need for extensive computation of superfluous high-frequency effects. Another advantage of AVM is that the resulting model is continuous and can therefore be linearized about any operating point. This allows for near-instantaneous calculation of transfer functions and/or frequency-domain characteristics.

The particular AVM approach used in the study is an extension of that used in [3]. This AVM method allows for the simulation of a system via parameters that are dependent upon

operating condition such as load impedance. In order to enhance the usefulness of this approach to a system with a controlled rectifier, it is extended by allowing for the characterization of the same parameters by firing angle (α) as well as operating condition.

Figure 8 shows a simple block diagram of the theoretical model. The inputs and output of the various blocks are shown, including the generator reference frame voltages and currents, $\overline{\boldsymbol{v}}_{qds}{}^{r}$ and $\bar{\boldsymbol{\imath}}_{qds}{}^{r}$, the rectifier output voltage, $\bar{v}_{out}$, and the load current, i_{load}. Similar to [3], the rectifier is modeled as an algebraic block with i_{load} and $\bar{\boldsymbol{\imath}}_{qds}{}^{r}$ as inputs and $\bar{v}_{out}$ and $\overline{\boldsymbol{v}}_{qds}{}^{r}$ as outputs. This allows for easy application of Park's equations and avoids numerous issues associated with using the generator voltages $\overline{\boldsymbol{v}}_{qds}{}^{r}$ as outputs of the generator model. The filter block includes the filter capacitance, C, filter inductance, L_f, the capacitor voltage, $\bar{v}_C$, and the rectifier output current, $\bar{\imath}_{out}$.

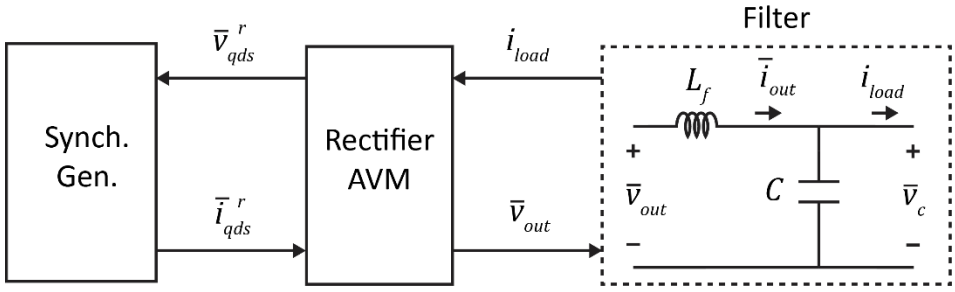

Figure 8. Block Diagram of Theoretical AVM Model

The model relies on the expression of synchronous machine equations in the rotor reference frame. The relationship between phase voltages and currents and their rotor-reference frame components can be highly variable due to load. This is remedied by the transformation of phase quantities into a synchronous reference frame so that they can be averaged. Specifically, it is useful to formulate a reference frame in which the average value *d*-axis component of the source input voltage is zero ($\bar{v}_{ds}{}^{*} = 0$). In [3] this is referred to as the rectifier reference frame, denoted by the superscript *rec*.

The relationship between the rotor and rectifier reference frame voltages is dependent upon the rotor position δ:

$$\begin{bmatrix} \bar{v}_{qs}{}^{rec} \\ 0 \end{bmatrix} = \begin{bmatrix} \cos(\delta) & \sin(\delta) \\ -\sin(\delta) & \cos(\delta) \end{bmatrix} \begin{bmatrix} \bar{v}_{qs}{}^{r} \\ \bar{v}_{ds}{}^{r} \end{bmatrix} \tag{26}$$

Linear algebraic functions are defined that relate machine variables in the rectifier reference frame $\overline{\boldsymbol{v}}_{qds}{}^{rec}$ and $\bar{\boldsymbol{\imath}}_{qds}{}^{rec}$ to the average converter output voltage and current.

$$\left\| \overline{\boldsymbol{v}}_{qds}{}^{rec} \right\| = \gamma(\cdot)\bar{v}_{out} \tag{27}$$

$$\bar{\imath}_{out} = \beta(\cdot)\left\| \bar{\boldsymbol{\imath}}_{qds}{}^{rec} \right\| \tag{28}$$

As proposed above, the functions $\gamma(\cdot)$ and $\beta(\cdot)$ are dependent upon both loading condition and firing angle. The loading condition may be defined by an impedance as calculated from parameters of the detailed simulation:

$$z = \frac{\bar{v}_c}{\left\| \bar{\imath}_{qds}{}^{r} \right\|} \tag{29}$$

One additional relationship is necessary to fully describe the rectifier, the angle between $\overline{\boldsymbol{v}}_{qds}{}^{rec}$ and $\bar{\boldsymbol{\imath}}_{qds}{}^{rec}$:

$$\varphi(\cdot) = \tan^{-1}\left(\frac{\bar{\imath}_{ds}{}^{r}}{\bar{\imath}_{qs}{}^{r}}\right) - \delta = \tan^{-1}\left(\frac{\bar{\imath}_{ds}{}^{r}}{\bar{\imath}_{qs}{}^{r}}\right) - \tan^{-1}\left(\frac{\bar{v}_{ds}{}^{r}}{\bar{v}_{qs}{}^{r}}\right) \tag{30}$$

The effect of the filter inductance L_F on the output impedance z is a concern for higher frequencies. To compensate it is necessary to relate the rectifier output voltage to the capacitor voltage:

$$v_{out} = v_C + H_L(s)i_{out} \tag{31}$$

where $H_L(s) = L_F s$. To avoid difficult computation in the time domain, $H_L(s)$ should be a proper transfer function; therefore, it can be approximated as such:

$$H_L(s) = \frac{L_F s}{\tau s + 1} \tag{32}$$

where τ is a time constant whose effect is negligible at the switching frequency. A value of 10 μs, as proposed in [3], is also used here.

The relationship between the load current and the rectifier output current is expressed as:

$$v_C = H_C(i_{out} - i_{load}) \tag{33}$$

where $H_C(s) = 1/(C_f s)$.

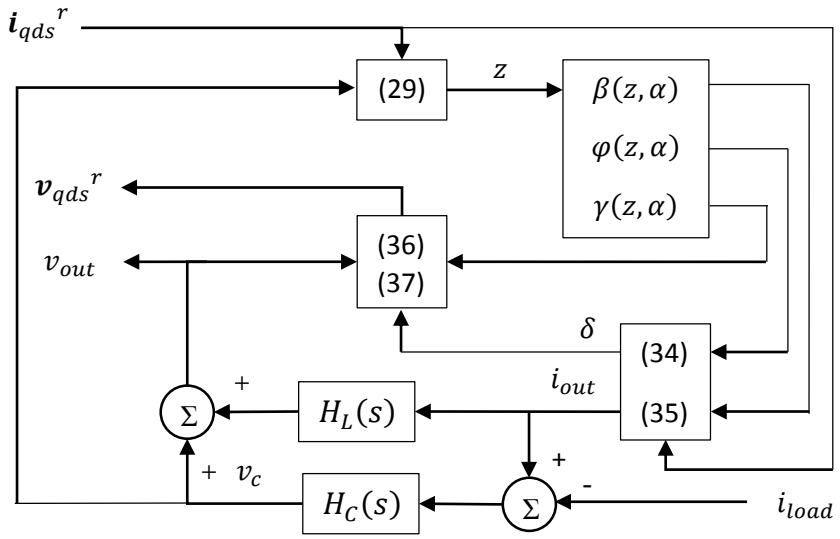

Figure 9. Block Diagram of AVM Rectifier Algebraic Block

The steps for implementation of the AVM are shown in **Figure 9**. The rectifier block uses $\bar{\imath}_{qds}{}^r$ as input from the machine model to calculate z with (29). Then, using z and firing angle α, the functions $\gamma(z,\alpha)$, $\beta(z,\alpha)$, and $\varphi(z,\alpha)$ are calculated. The rotor angle δ is calculated via (34):

$$\delta = \tan^{-1}\left(\frac{i_{ds}{}^r}{i_{qs}{}^r}\right) - \varphi(z,\alpha) \tag{34}$$

The rectifier output current is computed using

$$i_{out} = \beta(z,\alpha)\sqrt{\left({i_{qs}}^{r}\right)^2 + ({i_{ds}}^{r})^2} \tag{35}$$

Equation (31) is used to calculate the rectifier output voltage v_{out}, and the generator voltages ${v_{qs}}^{r}$ and ${v_{ds}}^{r}$ are calculated via (36) and (37):

$${v_{qs}}^{r} = \gamma(z,\alpha)v_{out}\cos\delta \tag{36}$$

$${v_{ds}}^{r} = \gamma(z,\alpha)v_{out}\sin\delta \tag{37}$$

3. LITERATURE REVIEW

There has been extensive work since at least the 1960s in using AVM techniques to simplify the simulation and modeling of power systems components [8]. The core concept of AVM techniques is to devise a simulation for switching components that retains accuracy and represents system dynamics without modeling each individual switching event. Many early studies developed reduced order AVMs with derivation of algebraic expressions and reference transformations applied to circuit models with constant voltage sources behind reactance, neglecting stator dynamics [9], [10], [11], [8]. The "Voltage-Behind-Reactance" model is formulated from the standard reduced-order model of the synchronous machine, relying on transient and sub-transient reactances jX_d' and jX_d'' to characterize the machine model, thus neglecting stator-winding transients [8] and leading the model to inaccurately represent fast electrical transients [9].

In [4], an average-value model of a three-phase fully-controlled rectifier is developed and analyzed in detail. This model represents the source as a voltage-behind-reactance but allows for accurate calculation of rectifier output voltage and *q* and *d*-axis source currents for changing input voltage amplitude and load current. The model utilizes a generator reference frame in which the *d*-axis voltage component is zero. Model inputs include the firing angle and *q* and *d*-axis components of the source voltage. The outputs include a fast average of the rectifier current and

q and *d*-axis components of the AC currents. The fast average values are valid so long as converter dynamics do not change dramatically within one averaging interval of $\frac{\pi}{3}$, consisting of the period of conduction for one thyristor. While this model is accurate for changes in source voltage amplitude and current, it assumes both Mode 1 operation and a constant commutating inductance, both of which make it inapplicable to generator-rectifier systems.

A generator-rectifier AVM using a reduced-order synchronous machine model is presented in [12]. This model represents the synchronous machine as equivalent circuits in the *q* and *d*-axes as opposed to the voltage-behind-reactance method. This approach yields additional terms in the average value equations, including commutating and transient inductances (L_c , L_t) that are dependent upon firing angle (β) and a term representing the voltage drop due to stator resistance in the dc output voltage equation (38).

$$\frac{3\sqrt{3E}}{\pi}\cos \propto -\frac{3}{\pi}\omega_r L_c\,(\beta)\bar{\imath}_{dc} - 2r_s\bar{\imath}_{dc} - L_t(\beta)p\bar{\imath}_{dc} \tag{38}$$

Although an improvement, this paper also considers only Mode 1 operation. A model valid for all modes is presented in [13], but this method utilizes a reduced-order machine model and requires the solving of a non-linear equation for each simulation step, likely increasing runtime.

In [14], a numerical model is proposed which extracts parameters from a detailed simulation of an uncontrolled generator-rectifier system to characterize its average behavior. This approach is refined in [3] by establishing lookup tables for AVM parameters that allow the model to accurately predict the system behavior over varying load conditions. This study uses an extension of the methods of [3], a numerical AVM based on parameters determined by an initial detailed simulation.. Here the AVM parameters are characterized based on two different variables, load and firing angle, thus yielding two-dimensional lookup tables for each parameter. The basic structure of the AVM and detailed models are based on [15], but with suitable

modifications in order to represent the physical system studied herein. These modifications, along with other work in characterizing the synchronous generator, make it possible to create a model of a particular generator-rectifier system and compare the model performance to the physical hardware.

4. SSFR GENERATOR CHARACTERIZATION

Standstill Frequency Response (SSFR) testing provides a simple and effective method of characterizing and modeling an electric machine, in this case a synchronous generator. This method enables one to determine machine parameters by extracting frequency response data from a machine at standstill and at voltages much less than the rated value. As such, it confers many advantages including decreased risk of damage to the machine, ability to identify the field response, increased safety for operators, and ease and economy of implementation.

A complete theoretical background of SSFR testing is not within the scope of this paper, but a summary sufficient to understand the method and its particular application in this work in provided. Many of the procedures and methods used for this study were adopted from IEEE Standard 115-1995 [16], [17]. Section 12 of this document describes a detailed procedure for performing SSFR testing on an electric machine. Numerous details of the documented method were modified in this case however, such as the decision of which functions to use for fitting measured data.

Stated simply, SSFR testing uses frequency response data from a machine at standstill, excited at low voltages, to determine parameters of rotor-reference-frame equivalent *d* and *q*-axis circuit models for a given electric machine.

The machine is modeled as a two-port network in the *d*-axis and a one port network in the *q*-axis. These models differ by order based on the number of damper windings used. Here the second order models were used for both direct and quadrature axes, including one damper winding in the *d*-axis model and two damper windings in the *q*-axis model.

The chosen models can be used to derive symbolic expressions for various transfer functions for the *d*-axis and *q*-axis networks in terms of their resistance and inductance

component values. These unknown R and L values constitute the set of parameters for a curve-fitting process to match the associated transfer function with corresponding measured data from the actual machine. Once an acceptable fit is found, the equivalent circuit models with their set of fitted parameters serves as a complete network model for the synchronous machine.

Typically *d*-axis measurements are performed first, requiring the machine to be aligned with the *d*-axis. This was done by shorting phases A and B, applying a small, 100 Hz sinusoidal excitation voltage across phases A and C with a signal generator, and monitoring the voltage at the open field terminals with an oscilloscope. The generator was then manually rotated until the observed voltage at the field terminals reached its minimum value.

Next the *d*-axis measurements were performed. These measurements can be categorized into three sets: (i) stator excitation with field shorted, (ii) stator excitation with field open, and (iii) field excitation with stator open (see **Figure 10**). An HP3567A signal analyzer was used in "Swept Sine" mode in combination with a Tektronix current probe to measure frequency response curves for various voltage-current ratio combinations. The following symbols define the measured voltages and currents:

$$V_{ab} = stator\ excitation\ voltage, phase\ a\ to\ b$$

$$I_a = stator\ current$$

$$V_{fd} = field\ excitation\ voltage$$

$$I_{fd} = field\ current$$

$$E_{ab} = stator\ emf, phase\ a\ to\ b$$

$$E_{fd} = field\ emf$$

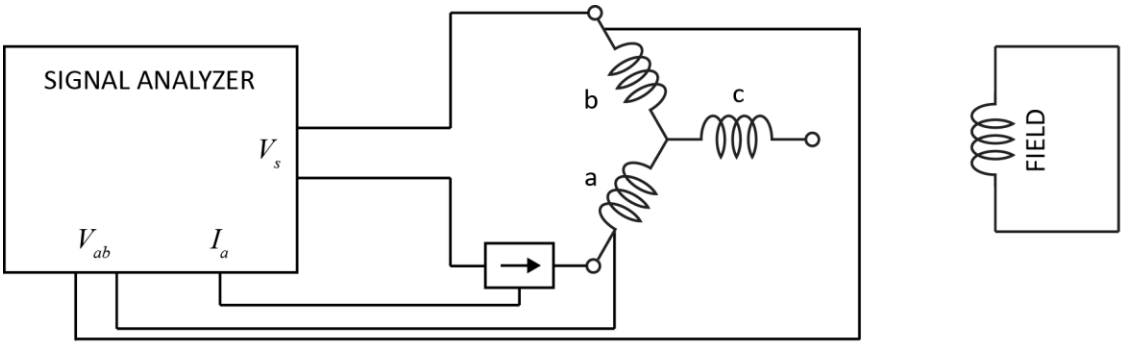

i) stator excitation with field shorted (Vab/Ia)

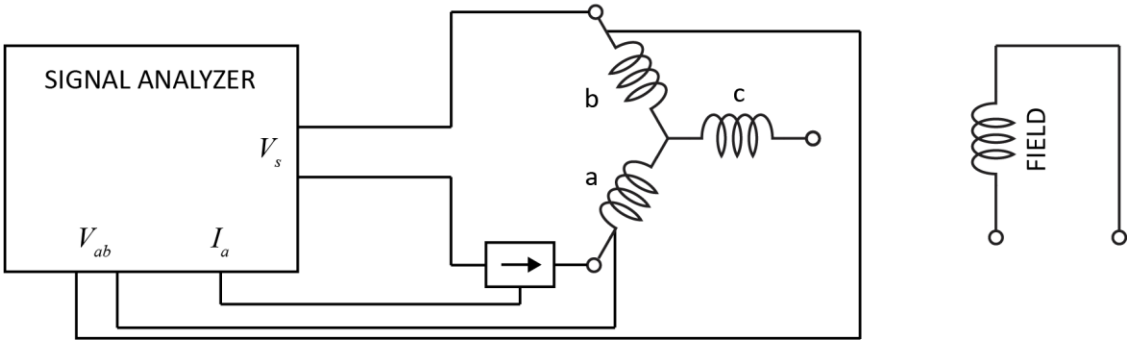

ii) stator excitation with field open (Vab/Ia)

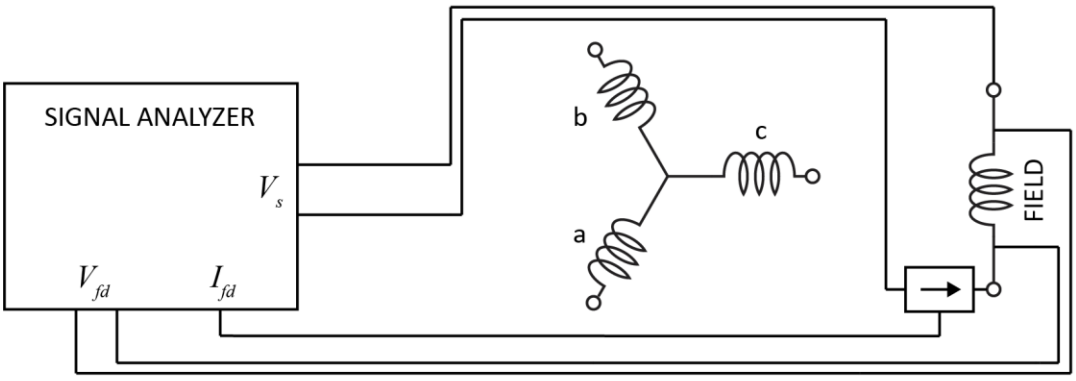

iii) field excitation with stator open (Vfd/Ifd)

Figure 10. Measurement Configuration for SSFR Data Collection

In terms of these symbols, the following transfer functions were measured for the *d*-axis. Also, the first transfer function (39) was measured for the *q*-axis. The subscript evaluations denote conditions of the setup or connections made during each measurement ($V_{fd} = 0$, field shorted; $I_{fd} = 0$, field open; $I_a = 0$, stator open).

$$\left.\frac{I_a}{V_{ab}}\right|_{V_{fd}=0} \tag{39}$$

$$\left.\frac{I_{fd}}{V_{ab}}\right|_{V_{fd}=0} \tag{40}$$

$$\left.\frac{I_a}{V_{ab}}\right|_{I_{fd}=0} \tag{41}$$

$$\left.\frac{E_{fd}}{V_{ab}}\right|_{I_{fd}=0} \tag{42}$$

$$\left.\frac{I_{fd}}{V_{fd}}\right|_{I_a=0} \tag{43}$$

$$\left.\frac{E_{ab}}{V_{fd}}\right|_{I_a=0} \tag{44}$$

After data collection several calculations were required to relate the measured quantities to the desired transfer functions used for fitting. These factors are introduced due to the reference frame transformation matrix $\boldsymbol{K}$ used to relate *q* and *d*-axis components in the equivalent circuit models of the machine to phase voltages at the machine terminals.

First the rotor angle is calculated for *d*-axis alignment. Recall that during the alignment procedure, phases a and b are shorted together ($V_{as} = V_{bs}$) (47), a voltage is applied from a to c (48), and the rotor is rotated such that the d-axis stator voltage is nulled (${V_{ds}}^r = 0$) (49).

$$\begin{bmatrix} {V_{qs}}^r \\ {V_{ds}}^r \end{bmatrix} = \frac{2}{3}\boldsymbol{K}\begin{bmatrix} V_{as} \\ V_{bs} \\ V_{cs} \end{bmatrix} \tag{45}$$

$$\begin{bmatrix} {V_{qs}}^r \\ {V_{ds}}^r \end{bmatrix} = \frac{2}{3}\begin{bmatrix} \cos(\theta_r) & \cos\left(\theta_r - \frac{2\pi}{3}\right) & \cos\left(\theta_r + \frac{2\pi}{3}\right) \\ \sin(\theta_r) & \sin\left(\theta_r - \frac{2\pi}{3}\right) & \sin\left(\theta_r + \frac{2\pi}{3}\right) \end{bmatrix}\begin{bmatrix} V_{as} \\ V_{bs} \\ V_{cs} \end{bmatrix} \quad (46)$$

$${V_{ds}}^r = \frac{2}{3}\begin{bmatrix} \sin(\theta_r) & \sin\left(\theta_r - \frac{2\pi}{3}\right) & \sin\left(\theta_r + \frac{2\pi}{3}\right) \end{bmatrix}\begin{bmatrix} V_{as} \\ V_{as} \\ V_{cs} \end{bmatrix} \quad (47)$$

$${V_{ds}}^r = \frac{2}{3}\begin{bmatrix} \sin(\theta_r) & \sin\left(\theta_r - \frac{2\pi}{3}\right) & \sin\left(\theta_r + \frac{2\pi}{3}\right) \end{bmatrix}\begin{bmatrix} V_{as} - V_{cs} \\ V_{as} - V_{cs} \\ V_{cs} - V_{cs} \end{bmatrix} \quad (48)$$

$$0 = V_{ac}\frac{2}{3}\left[\sin(\theta_r) + \sin\left(\theta_r - \frac{2\pi}{3}\right)\right] \quad (49)$$

$$\sin(\theta_r) = -\sin\left(\theta_r - \frac{2\pi}{3}\right) \quad (50)$$

$$\theta_r = \frac{\pi}{3}, -\frac{2\pi}{3} \quad (51)$$

Next, the relationship between the *d*-axis stator voltage and the input voltage can be calculated for tests performed with stator excitation. For these tests, voltage is applied at the machine terminals between a and b, c is left open ($V_{cs} = 0$) (52), and the machine is aligned with the *d*-axis ($\theta_r = \frac{\pi}{3}$).

$${V_{ds}}^r = \frac{2}{3}\begin{bmatrix} \sin(\theta_r) & \sin\left(\theta_r - \frac{2\pi}{3}\right) & \sin\left(\theta_r + \frac{2\pi}{3}\right) \end{bmatrix}\begin{bmatrix} V_{as} \\ V_{bs} \\ 0 \end{bmatrix} \quad (52)$$

$${V_{ds}}^r = \frac{2}{3}\begin{bmatrix} \sin(\theta_r) & \sin\left(\theta_r - \frac{2\pi}{3}\right) \end{bmatrix}\begin{bmatrix} V_{as} - V_{bs} \\ V_{bs} - V_{bs} \end{bmatrix} (53)$$

$${V_{ds}}^r = \frac{2}{3}\begin{bmatrix} \sin(\theta_r) & \sin\left(\theta_r - \frac{2\pi}{3}\right) \end{bmatrix}\begin{bmatrix} V_{ab} \\ 0 \end{bmatrix} \quad (54)$$

$${V_{ds}}^r = \frac{2}{3}V_{ab} * \sin(\theta_r) \quad (55)$$

$${V_{ds}}^r = \pm\frac{1}{\sqrt{3}}V_{ab} \quad (56)$$

A similar relation can be derived for the current (assume $I_{cs} = 0$, $I_{bs} = -I_{as}$, and, $\theta_r = \frac{\pi}{3}$ when aligned with the *d*-axis):

$$I_{ds}{}^{r} = \frac{2}{3}\begin{bmatrix}\sin(\theta_r) & \sin\left(\theta_r - \frac{2\pi}{3}\right) & \sin\left(\theta_r + \frac{2\pi}{3}\right)\end{bmatrix}\begin{bmatrix}I_{as}\\ I_{bs}\\ I_{cs}\end{bmatrix} \tag{57}$$

$$I_{ds}{}^{r} = \frac{2}{3}\begin{bmatrix}\sin(\theta_r) & \sin\left(\theta_r - \frac{2\pi}{3}\right) & \sin\left(\theta_r + \frac{2\pi}{3}\right)\end{bmatrix}\begin{bmatrix}I_{as}\\ -I_{as}\\ 0\end{bmatrix} \tag{58}$$

$$I_{ds}{}^{r} = \frac{2}{3}\left(\sin(\theta_r) - \sin\left(\theta_r - \frac{2\pi}{3}\right)\right)I_{as} \tag{59}$$

$$I_{ds}{}^{r} = \pm\frac{2}{\sqrt{3}}I_{as} \tag{60}$$

It is also necessary to relate the measured field quantities to the equivalent circuit field quantities via a turns ratio:

$$V'_{fd} = \frac{N_s}{N_{fd}}V_{fd} \tag{61}$$

$$I'_{fd} = \frac{2}{3}\frac{N_{fd}}{N_s}I_{fd} \tag{62}$$

The rotor angle for *q*-axis alignment was calculated by solving the rotor-reference equation for the configuration used during *q*-axis alignment. Alignment to the *q*-axis was done by applying a voltage at the machine terminals from a to b with c open. The rotor was then rotated until the observed rotor voltage was nulled or minimized. This was determined by measuring the transfer function of the rotor voltage to input voltage ratio at frequencies around 100 Hz. Successive trials were repeated until the lowest dB magnitude response was achieved, thus

measuring the minimum rotor voltage. The calculations assume that $I_{bs} = -I_{as}$, $I_{cs} = 0$ and, when aligned, ${I_{ds}}^{r} = 0$.

$${I_{ds}}^{r} = \frac{2}{3}\left[\sin(\theta_r) \quad \sin\left(\theta_r - \frac{2\pi}{3}\right) \quad \sin\left(\theta_r + \frac{2\pi}{3}\right)\right]\begin{bmatrix} I_{as} \\ I_{bs} \\ I_{cs} \end{bmatrix} \tag{63}$$

$$0 = \frac{2}{3}\left[\sin(\theta_r) \quad \sin\left(\theta_r - \frac{2\pi}{3}\right) \quad \sin\left(\theta_r + \frac{2\pi}{3}\right)\right]\begin{bmatrix} I_{as} \\ -I_{as} \\ 0 \end{bmatrix} \tag{64}$$

$$0 = \frac{2}{3}\left(\sin(\theta_r) - \sin\left(\theta_r - \frac{2\pi}{3}\right)\right) I_{as} \tag{65}$$

$$\sin(\theta_r) = \sin\left(\theta_r - \frac{2\pi}{3}\right) \tag{66}$$

$$\theta_r = \frac{5\pi}{6} \pm \pi \tag{67}$$

Given the *q*-axis rotor angle, $\theta_r = \frac{5\pi}{6} \pm \pi$, the relationship between the measured input voltage for the *q*-axis test and the *q*-axis equivalent circuit quantity can be calculated.

$${V_{qs}}^{r} = \frac{2}{3}\left[\cos(\theta_r) \quad \cos\left(\theta_r - \frac{2\pi}{3}\right) \quad \cos\left(\theta_r + \frac{2\pi}{3}\right)\right]\begin{bmatrix} V_{as} - V_{bs} \\ V_{bs} - V_{bs} \\ V_{cs} - V_{bs} \end{bmatrix} \tag{68}$$

$${V_{qs}}^{r} = \frac{2}{3}\left[\cos\left(\frac{5\pi}{6}\right) \quad \cos\left(\frac{5\pi}{6} - \frac{2\pi}{3}\right) \quad \cos\left(\frac{5\pi}{6} + \frac{2\pi}{3}\right)\right]\begin{bmatrix} V_{ab} \\ 0 \\ V_{cb} \end{bmatrix} \tag{69}$$

$${V_{qs}}^{r} = \frac{2}{3}\left[\cos\left(\frac{5\pi}{6}\right) \quad \cos\left(\frac{5\pi}{6} - \frac{2\pi}{3}\right) \quad 0\right]\begin{bmatrix} V_{ab} \\ 0 \\ V_{cb} \end{bmatrix} \tag{70}$$

$${V_{qs}}^{r} = \frac{2}{3}\cos\left(\frac{5\pi}{6}\right) V_{ab} \tag{71}$$

$${V_{qs}}^{r} = \pm\frac{1}{\sqrt{3}} V_{ab} \tag{72}$$

In addition to relating the *q* and *d*-axis equivalent circuit quantities to their measured counterparts, it is necessary to derive equations for the desired transfer functions of the *q* and *d*-axis equivalent circuits. These transfer functions are symbolic expressions in terms of the unknown equivalent circuit parameters. For the sake of brevity and legibility, these equations are presented in terms of the following impedances and reactances:

Table 2. Q-Axis and D-Axis Equivalent Circuit Parameter Definitions

$\boldsymbol{Z_{sd}}$	$\boldsymbol{r_s}$	stator impedance
$\boldsymbol{jX_{md}}$	$j\omega L_{md}$	*d*-axis magnetizing branch reactance
$\boldsymbol{Z'_{kd}}$	$r'_{kd} + j\omega L'_{lkd}$	referred *d*-axis field damper winding impedance
$\boldsymbol{Z'_{fd}}$	$r'_{fd} + j\omega L'_{lfd}$	referred *d*-axis field impedance
$\boldsymbol{Z'_{kq1}}$	$r'_{kq1} + j\omega L'_{lkq1}$	referred *q*-axis primary damper winding impedance
$\boldsymbol{Z'_{kq2}}$	$r'_{kq2} + j\omega L'_{lkq2}$	referred *q*-axis secondary damper winding impedance

The impedances listed consist of complex pairs of resistance and reactance, with associated R and L values as parameters of the fitting process. The *d*-axis and *q*-axis equivalent circuits can be seen in **Figure 11** and **Figure 12**, respectively.

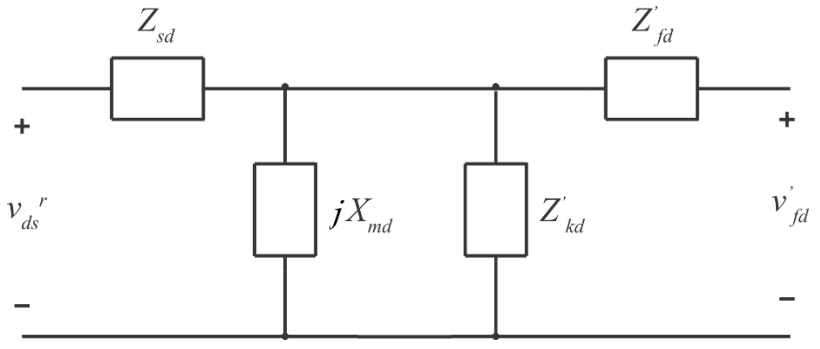

Figure 11. D-axis Equivalent Circuit Model

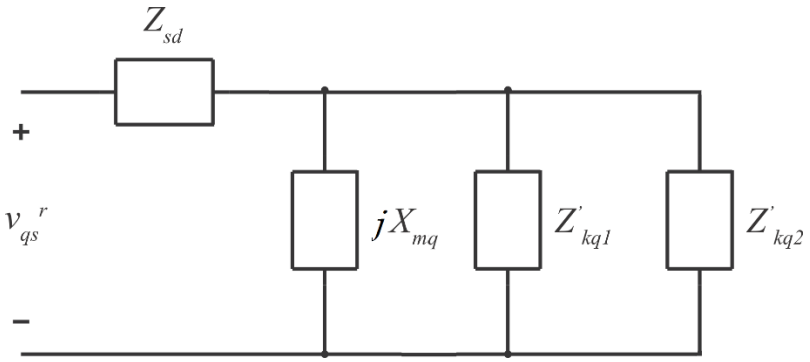

Figure 12. Q-axis Equivalent Circuit Model

The following transfer functions, in terms of the equivalent circuit parameters, were then derived. The equations are written here in terms of equivalent circuit impedances and reactances and using the symbol || to denote a parallel combination of impedance and/or reactance.

$$\left.\frac{V_{ds}{}^{r}}{I_{ds}{}^{r}}\right|_{V'_{fd}=0} = Z_{sd} + jX_{md} \| Z'_{kd} \| Z'_{fd} \tag{73}$$

$$\left.\frac{I'_{fd}}{I_{ds}{}^{r}}\right|_{V'_{fd}=0} = \frac{jX_{md} \| Z'_{kd}}{Z'_{fd} + jX_{md} \| Z'_{kd}} \tag{74}$$

$$\left.\frac{V_{ds}{}^{r}}{I_{ds}{}^{r}}\right|_{I'_{fd}=0} = Z_{sd} + jX_{md} \| Z'_{kd} \tag{75}$$

$$\left.\frac{V'_{fd}}{I_{ds}{}^{r}}\right|_{I'_{fd}=0} = X_{md} \| Z'_{kd} \tag{76}$$

$$\left.\frac{V'_{fd}}{I'_{fd}}\right|_{I_{ds}{}^{r}=0} = Z'_{fd} + jX_{md} \| Z'_{kd} \tag{77}$$

$$\left.\frac{V_{ds}{}^{r}}{I'_{fd}}\right|_{I_{ds}{}^{r}=0} = jX_{md} \| Z'_{kd} \tag{78}$$

$$\left.\frac{V_{qs}{}^{r}}{I_{qs}{}^{r}}\right|_{V'_{fd}=0} = Z_{sd} + jX_{md} \| Z'_{kq1} \| Z'_{kq2} \tag{79}$$

The measured transfer functions were then used to calculate transfer functions corresponding to those listed above, and the data was scaled using the calculated constants in

the relations above. After these steps, the measured data was ready to be fitted to the equivalent circuit transfer functions.

For fitting, the Genetic Optimization System Engineering Toolbox (Version 2.4), or GOSET, was used. This MATLAB toolset allowed the transfer functions to be fit to the measured data for a common set of circuit parameters by using a genetic algorithm.

An important component to fitting the data is the selection of a good fitness function, an expression that quantifies the error between the measured and calculated data. This function will determine which data is important for the accuracy or fitness of the model. In this case, a determination was made to prioritize transfer function magnitude over phase in fitting. The fitness function code is provided in the appendix for reference. The data, while measured up to 10kHz, was only fitted to 1kHz.

This process provides one set of parameters which fit to all of the above transfer functions, thus defining an acceptable model of the *q*-axis and *d*-axis equivalent networks for the synchronous generator. The results of the fitting process are seen in **Figure 13**, as well as the equivalent circuit parameters derived in **Table 3**. The magnitude and phase graphs labeled (a)–(g) correspond to the transfer functions of equations (73)– (79).

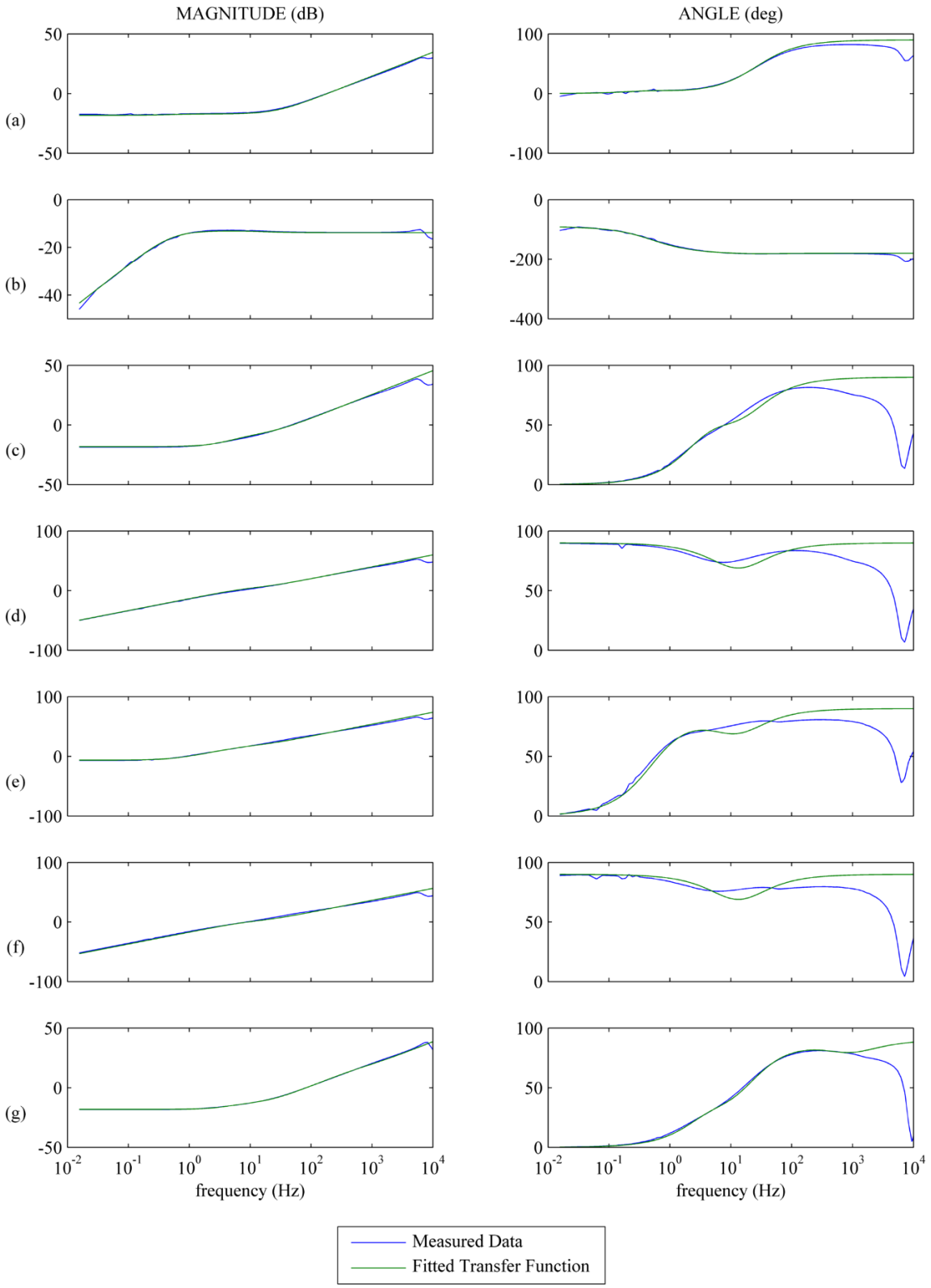

Figure 13. SSFR GA Fitting Results: (a) $V_{ds}{}^{r}/I_{ds}{}^{r}|_{V'_{fd}=0}$; (b) $I'_{fd}/I_{ds}{}^{r}\big|_{V'_{fd}=0}$; (c) $V_{ds}{}^{r}/I_{ds}{}^{r}|_{I'_{fd}=0}$; (d) $V'_{fd}/I_{ds}{}^{r}\big|_{I'_{fd}=0}$; (e) $V'_{fd}/I'_{fd}\big|_{I_{ds}{}^{r}=0}$; (f) $V_{ds}{}^{r}/I'_{fd}\big|_{I_{ds}{}^{r}=0}$; (g) $V_{qs}{}^{r}/I_{qs}{}^{r}\big|_{V'_{fd}=0}$

Table 3. Equivalent Circuit Parameter Values for SSFR Generator Model

r_s	0.1235
r'_{fd}	0.0212
r'_{kd}	0.6187
r'_{kq1}	0.2380
r'_{kq2}	23.4910
L_{ls}	0.0003
L_{md}	0.0057
L_{mq}	0.0034
L'_{lfd}	0.0007
L'_{lkd}	0.0051
L'_{lkq1}	0.0029
L'_{lkq2}	0.0031
N_s/N_{fd}	0.1709

5. PARAMETER EXTRACTION FROM DETAILED MODEL

Detailed Model Structure

The detailed model used for parameter extraction (**Figure 14**) was built in Matlab/Simulink using the ASMG for Simulink software package. With the exception of the Firing block (**Figure 15**) and the Controlled Rectifier Block (**Figure 16**) the model consists of standard ASMG components and blocks, including the Three Phase Synchronous Machine.

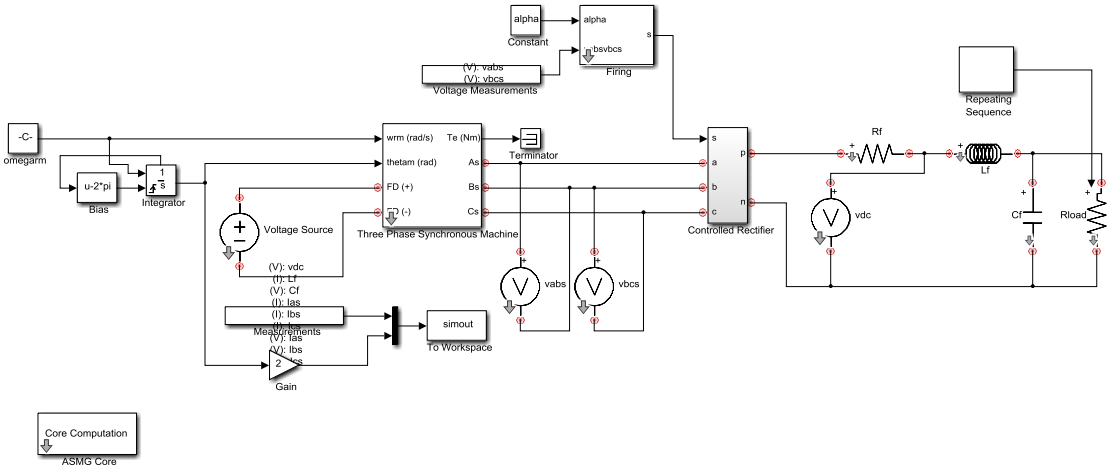

Figure 14. Detailed Synchronous-Generator/Controlled-Rectifier System Simulation Model for Matlab/Simulink

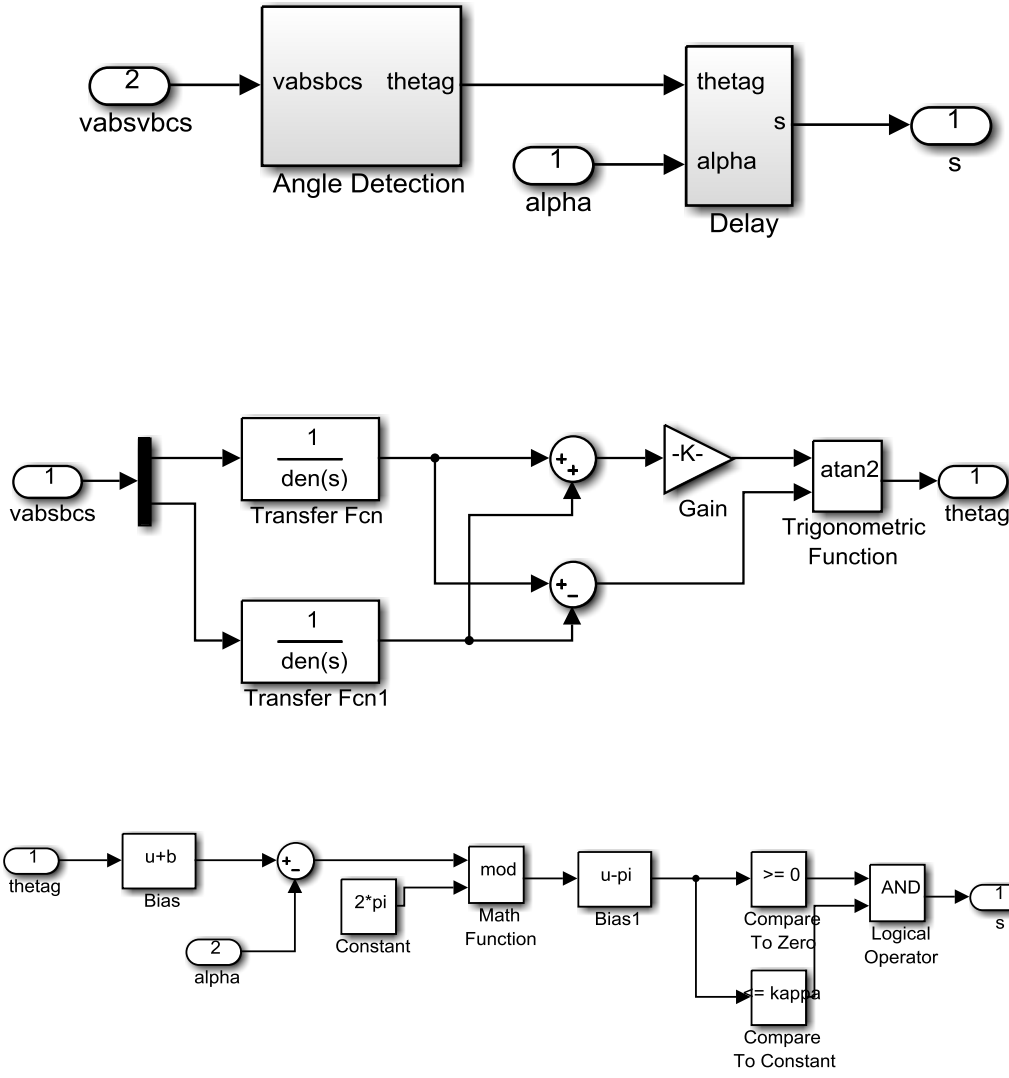

Figure 15. Firing Block, Angle Detection, and Delay sub-models of Detailed Model

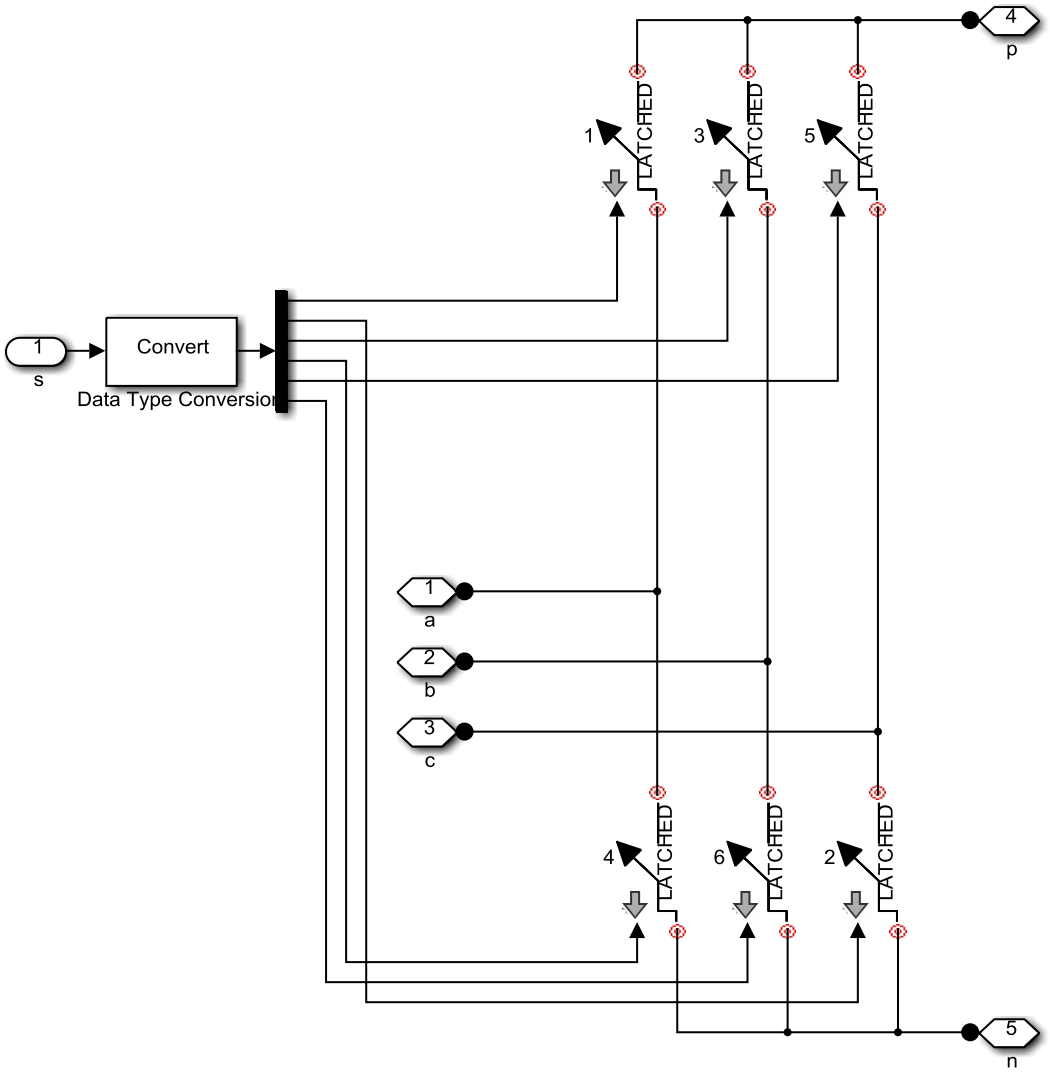

Figure 16. Controlled Rectifier sub-model of Detailed Model

The controlled rectifier block simply consists of switches that are activated by firing commands from the Firing block. The Firing block determines the timing of gating pulses for all six switches based on the delay angle input alpha. This discussion is mostly derived from [15]. First, the angle at which firing begins, defined here as θ_g, can be calculated from measurements of line-to-line voltages.

If we assume the line-to-neutral voltage to be

$$v_{as} = \sqrt{2}E\cos(\theta_g) \tag{80}$$

where E is the line-to-neutral rms voltage, then thyristor T1 should begin firing when $\theta_g = -\pi/3 + \alpha$, with thyristors T2 through T6 firing successively each $\pi/3$ radians. Given (80), the line-to-line voltages v_{abs} and v_{bcs} are represented as follows for a balanced set:

$$v_{abs} = \sqrt{6}E\cos\left(\theta_g + \frac{\pi}{6}\right) \tag{81}$$

$$v_{bcs} = \sqrt{6}E\cos\left(\theta_g - \frac{\pi}{2}\right) \tag{82}$$

These voltages are then filtered in order to induce a phase delay of $\pi/3$. Given the filter transfer function

$$H_f(s) = \frac{1}{\tau s+1} \tag{83}$$

the time constant to yield such a delay can be determined by solving the following equation:

$$\angle H_f(j2\pi 60) = \tan^{-1}\tau 2\pi 60 = \frac{\pi}{3} \tag{84}$$

The filtered voltage measurements are expressed as

$$v_{abs}{}^f = \sqrt{6}E_f\cos\left(\theta_g + \frac{\pi}{6}\right) \tag{85}$$

$$v_{bcs}{}^f = \sqrt{6}E_f\cos\left(\theta_g - \frac{5\pi}{6}\right) \tag{86}$$

where E_f is E times the filter magnitude $\left|H_f(s)\right|$. Calculating the sum and difference of the filtered values eliminates the phase shifts in each

$$v_{abs}{}^f + v_{bcs}{}^f = \sqrt{6}E_f\sin(\theta_g) \tag{87}$$

$$v_{abs}{}^f - v_{bcs}{}^f = \sqrt{6}E_f\sqrt{3}\cos(\theta_g) \tag{88}$$

Solving each for its respective sine or cosine, an expression for $\tan(\theta_g)$ is formulated. The arctangent yields an expression for θ_g:

$$\theta_g = \tan^{-1} \frac{\sqrt{3}(v_{abs}{}^f + v_{bcs}{}^f)}{v_{abs}{}^f - v_{bcs}{}^f} \tag{89}$$

Once θ_g is known, an algorithm calculates the angle at which successive thyristors will be fired.

AVM Parameter Extraction

The detailed model is run for values in z and α to determine the AVM parameters γ, β, and φ for a wide range of operating conditions, thus providing sufficient characterization data for the AVM. The rotor speed is assumed to be a constant 1800 rpm, corresponding to the physical generator studied herein, a four-pole synchronous generator operating at 60 Hz. The field voltage for the detailed model is assumed to be a constant value of 19.5V. For the filter inductor, a series resistance of 150 mΩ was used. This value is consistent with measurements of the inductor series resistance performed for relevant operating frequencies.

For parameter extraction, the series of impedance values chosen comprised a semi-logarithmic distribution ranging from 100 Ω to 0.01 Ω. This range was chosen to represent a wide range of possible loading conditions for the converter. Likewise, a series of values for α was chosen to be the following: 0, π/12, π/6, π/4, π/3, 5π/12, and π/2 radians. The simulation executes by stepping the load between values of z every three seconds to allow the output to reach steady state while holding α constant. This is then repeated for all listed values of the firing angle.

After completion, data from the simulation is used to determine the functions $\gamma(z, \alpha)$, $\beta(z, \alpha)$, and $\varphi(z, \alpha)$ via numerical averaging of respective voltages and currents over one switching interval. After the value of these functions is determined for each firing angle and impedance value, the points are used to define lookup tables for each function. These support points form the basis for interpolated 2-D lookup tables which are used in the AVM model. The

functions are visualized below as surface plots and the function support points are listed in the following tables.

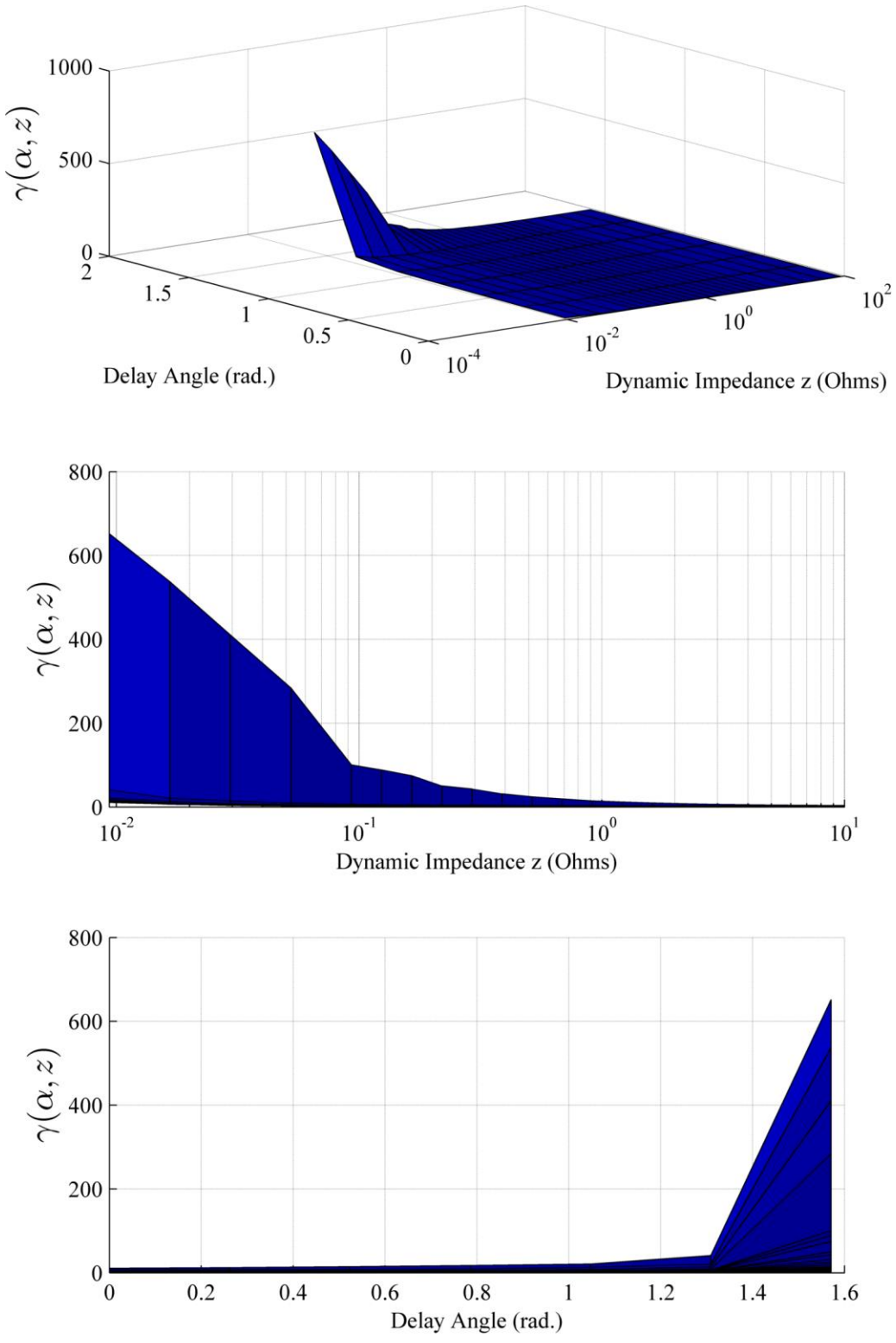

Figure 17. Function $\gamma(z, \alpha)$

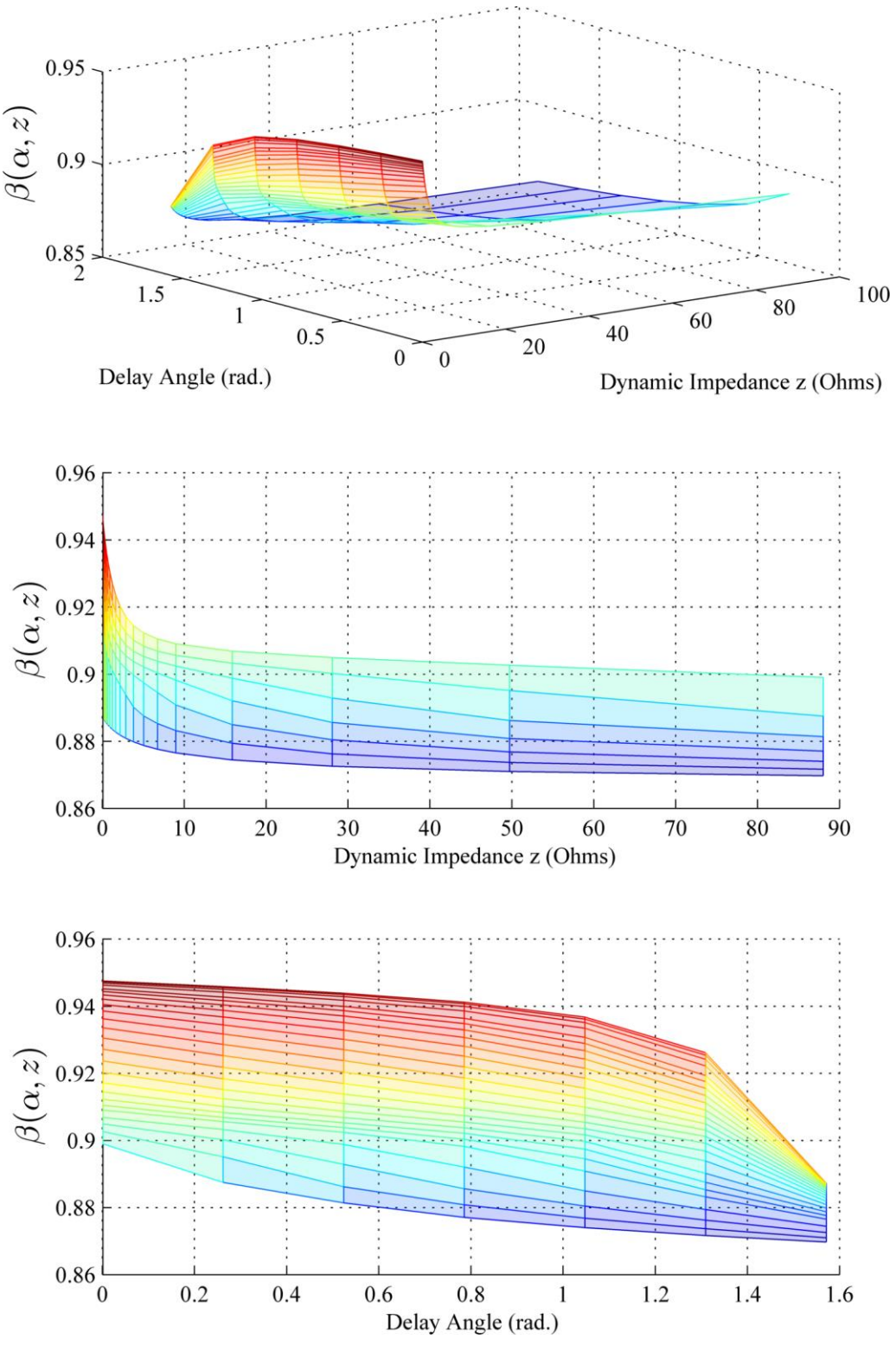

Figure 18. Function $\beta(z, \alpha)$

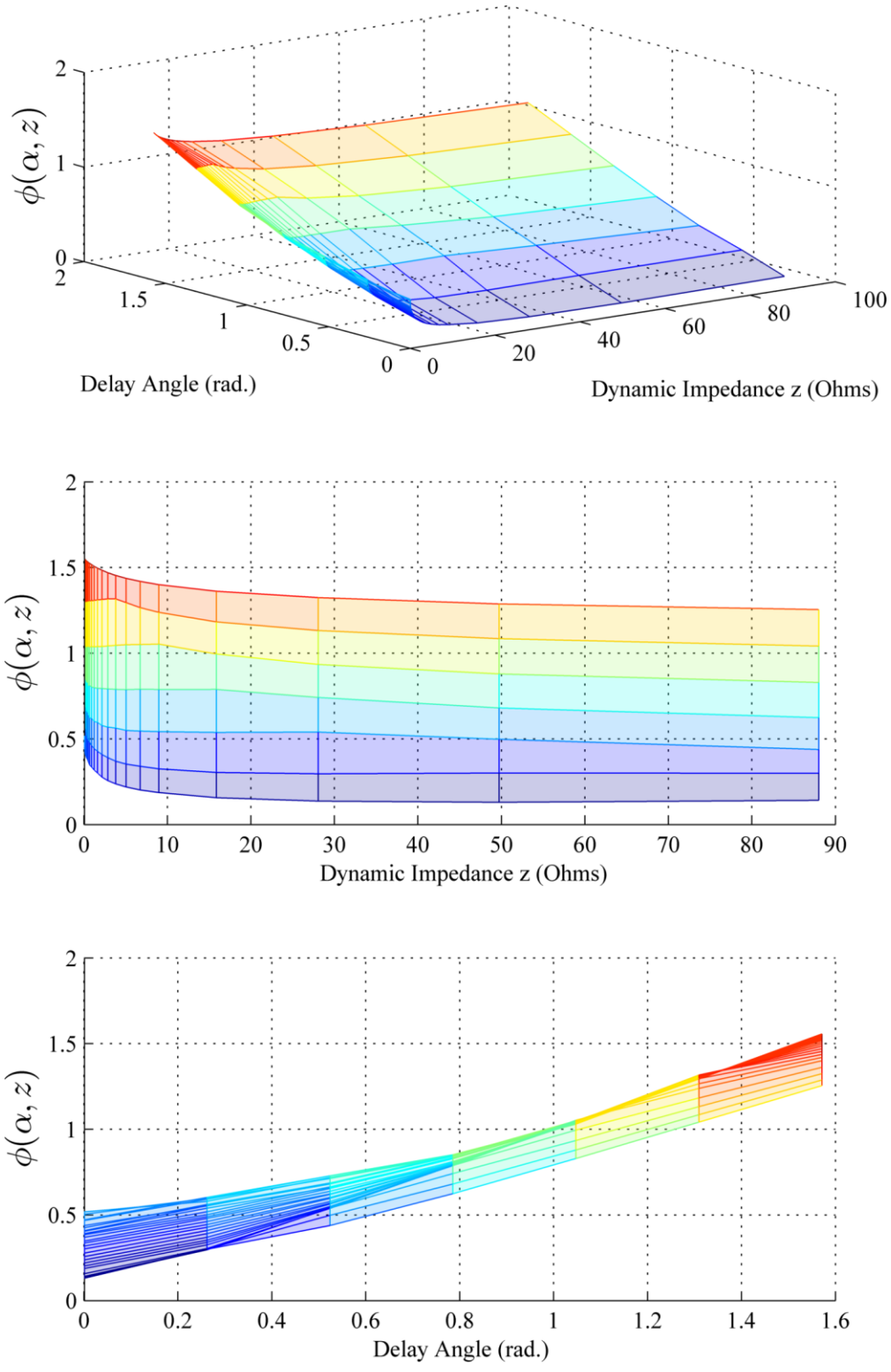

Figure 19. Function $\varphi(z, \alpha)$

Table 4. Support Points for $\gamma(z, \alpha)$

z \ α	0	π/12	π/6	π/4	π/3	5π/12	π/2
0.0094	10.8366	12.2203	14.4013	16.9544	20.6781	40.7791	651.9421
0.0166	7.1813	6.9982	7.9502	9.0859	12.9690	20.4080	537.7586
0.0295	4.0397	4.3621	4.8617	5.4764	7.3806	14.0134	410.6644
0.0523	2.6743	2.8819	3.1696	3.4517	4.8430	8.9087	284.3722
0.0929	1.7998	1.9090	2.0486	2.4847	3.2924	6.2701	100.5427
0.1237	1.4980	1.6224	1.7403	2.0792	2.7034	5.2885	88.7146
0.1647	1.2888	1.3819	1.5162	1.7794	2.3680	4.4840	74.7572
0.2192	1.1372	1.2089	1.3132	1.5594	2.0393	4.0788	50.2113
0.2917	1.0153	1.0825	1.1909	1.3963	1.8520	3.7517	43.0170
0.3880	0.9277	0.9797	1.0818	1.2755	1.7094	3.3544	31.5789
0.5161	0.8583	0.9057	0.9997	1.1628	1.6017	3.1568	24.3081
0.6863	0.8037	0.8520	0.9301	1.1009	1.4913	2.9371	19.1604
0.9126	0.7641	0.8067	0.8888	1.0406	1.4378	2.8602	14.5747
1.2135	0.7322	0.7690	0.8433	0.9974	1.3782	2.7458	12.0838
1.6137	0.7060	0.7405	0.8161	0.9666	1.3359	2.6609	9.7112
2.1462	0.6846	0.7157	0.7846	0.9449	1.3069	2.6119	7.7727
2.8549	0.6676	0.6962	0.7653	0.9202	1.2868	2.5754	6.5741
3.7979	0.6539	0.6806	0.7504	0.9008	1.2729	2.5073	5.5267
5.0540	0.6433	0.6676	0.7340	0.8853	1.2473	2.2646	4.7366
6.7260	0.6345	0.6581	0.7236	0.8796	1.2419	2.0445	4.0717
8.9505	0.6274	0.6502	0.7181	0.8673	1.2368	1.8534	3.6146
15.8499	0.6183	0.6378	0.7078	0.8579	1.1061	1.5890	2.9098
28.0639	0.6127	0.6325	0.7002	0.8107	1.0020	1.3930	2.4259
49.6926	0.6093	0.6276	0.6775	0.7614	0.9281	1.2611	2.1184
87.9915	0.6072	0.6226	0.6536	0.7245	0.8688	1.1627	1.8818

Table 5. Support Points for $\beta(z, \alpha)$

z \ α	0	π/12	π/6	π/4	π/3	5π/12	π/2
0.0094	0.9475	0.9458	0.9438	0.9412	0.9367	0.9261	0.8873
0.0166	0.9473	0.9455	0.9434	0.9407	0.9361	0.9254	0.8872
0.0295	0.9469	0.9450	0.9428	0.9399	0.9351	0.9241	0.8872
0.0523	0.9462	0.9441	0.9417	0.9385	0.9334	0.9222	0.8871
0.0929	0.9451	0.9427	0.9399	0.9363	0.9307	0.9193	0.8869
0.1237	0.9443	0.9416	0.9386	0.9348	0.9288	0.9175	0.8868
0.1647	0.9433	0.9403	0.9370	0.9329	0.9267	0.9155	0.8866
0.2192	0.9420	0.9387	0.9351	0.9306	0.9242	0.9133	0.8864
0.2917	0.9405	0.9367	0.9328	0.9280	0.9214	0.9111	0.8861
0.3880	0.9385	0.9344	0.9301	0.9251	0.9185	0.9090	0.8858
0.5161	0.9362	0.9317	0.9270	0.9219	0.9155	0.9069	0.8854
0.6863	0.9335	0.9286	0.9237	0.9186	0.9126	0.9049	0.8848
0.9126	0.9305	0.9252	0.9203	0.9153	0.9099	0.9030	0.8842
1.2135	0.9271	0.9217	0.9169	0.9123	0.9075	0.9012	0.8835
1.6137	0.9237	0.9183	0.9138	0.9096	0.9054	0.8991	0.8827
2.1462	0.9203	0.9151	0.9110	0.9074	0.9035	0.8968	0.8818
2.8549	0.9171	0.9124	0.9087	0.9054	0.9016	0.8938	0.8809
3.7979	0.9145	0.9101	0.9068	0.9037	0.8997	0.8902	0.8798
5.0540	0.9122	0.9083	0.9052	0.9021	0.8974	0.8875	0.8787
6.7260	0.9105	0.9068	0.9038	0.9003	0.8945	0.8853	0.8776
8.9505	0.9090	0.9056	0.9024	0.8982	0.8908	0.8832	0.8765
15.8499	0.9068	0.9032	0.8988	0.8920	0.8850	0.8794	0.8744
28.0639	0.9049	0.9002	0.8929	0.8856	0.8804	0.8762	0.8726
49.6926	0.9026	0.8951	0.8862	0.8808	0.8768	0.8737	0.8710
87.9915	0.8990	0.8875	0.8814	0.8771	0.8740	0.8717	0.8697

Table 6. Support Points for $\varphi(z, \alpha)$

z \ α	0	π/12	π/6	π/4	π/3	5π/12	π/2
0.0094	0.5180	0.5793	0.7184	0.8463	1.0499	1.2952	1.5564
0.0166	0.5041	0.5967	0.7287	0.8516	1.0387	1.2927	1.5559
0.0295	0.4713	0.6025	0.7282	0.8473	1.0305	1.2949	1.5549
0.0523	0.4672	0.5926	0.7127	0.8453	1.0417	1.2945	1.5532
0.0929	0.4377	0.5526	0.6858	0.8498	1.0434	1.2962	1.5516
0.1237	0.4252	0.5610	0.6866	0.8437	1.0337	1.2956	1.5494
0.1647	0.4081	0.5541	0.6804	0.8425	1.0402	1.2962	1.5468
0.2192	0.4044	0.5395	0.6595	0.8347	1.0300	1.2991	1.5444
0.2917	0.3912	0.5188	0.6639	0.8302	1.0332	1.3002	1.5400
0.3880	0.3848	0.5015	0.6545	0.8279	1.0375	1.3005	1.5359
0.5161	0.3696	0.4898	0.6383	0.8093	1.0382	1.3031	1.5307
0.6863	0.3475	0.4802	0.6225	0.8120	1.0354	1.3044	1.5241
0.9126	0.3363	0.4616	0.6198	0.8029	1.0383	1.3059	1.5171
1.2135	0.3185	0.4437	0.6023	0.7987	1.0371	1.3076	1.5071
1.6137	0.3015	0.4279	0.5965	0.7955	1.0383	1.3110	1.4963
2.1462	0.2772	0.4094	0.5783	0.7943	1.0387	1.3132	1.4845
2.8549	0.2567	0.3908	0.5688	0.7916	1.0424	1.3167	1.4694
3.7979	0.2378	0.3699	0.5633	0.7891	1.0456	1.3167	1.4537
5.0540	0.2195	0.3531	0.5496	0.7875	1.0494	1.2950	1.4364
6.7260	0.2021	0.3403	0.5457	0.7899	1.0506	1.2657	1.4191
8.9505	0.1871	0.3255	0.5426	0.7886	1.0531	1.2383	1.3999
15.8499	0.1571	0.3045	0.5381	0.7889	0.9952	1.1826	1.3613
28.0639	0.1372	0.2966	0.5402	0.7418	0.9344	1.1321	1.3242
49.6926	0.1304	0.3010	0.4980	0.6807	0.8791	1.0848	1.2875
87.9915	0.1417	0.2998	0.4383	0.6242	0.8292	1.0416	1.2545

6. AVM SIMULATION MODEL

The AVM simulation model was implemented in Matlab/Simulink. The top level model is seen in **Figure 20**. The model is configured here with constant *alpha* and a step load change.

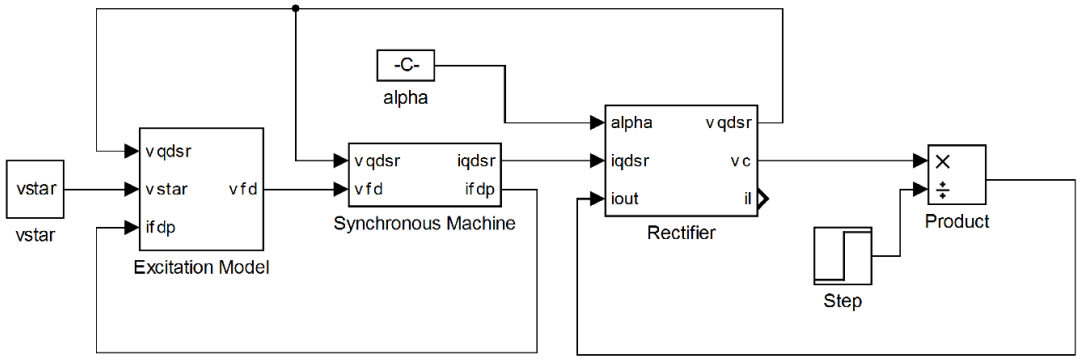

Figure 20. Top-level Simulink AVM Simulation Model

The standard synchronous machine model is shown in **Figure 21**, with sub-models for the Flux Linkage Dynamics in **Figure 22** and Currents in **Figure 23**.

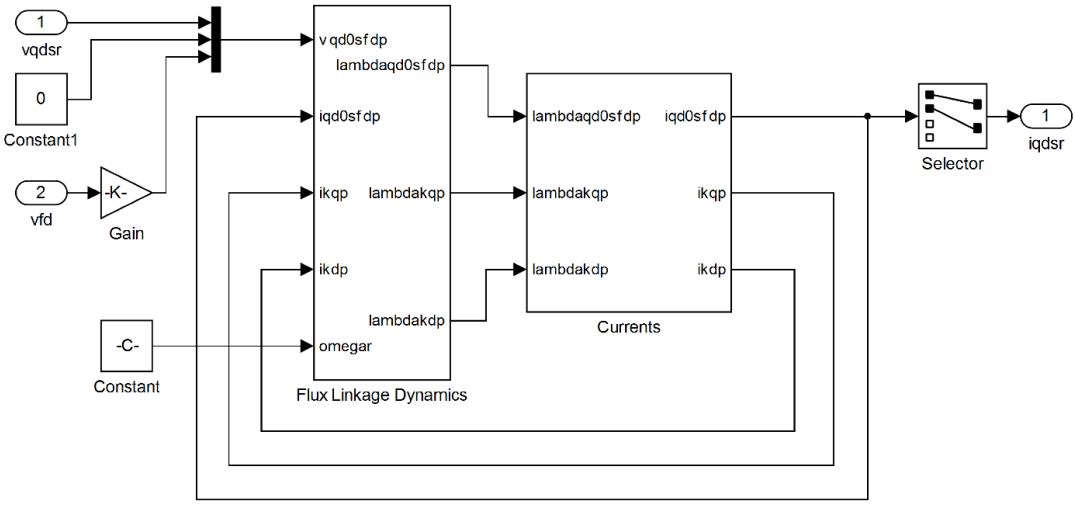

Figure 21. AVM Synchronous Machine Model

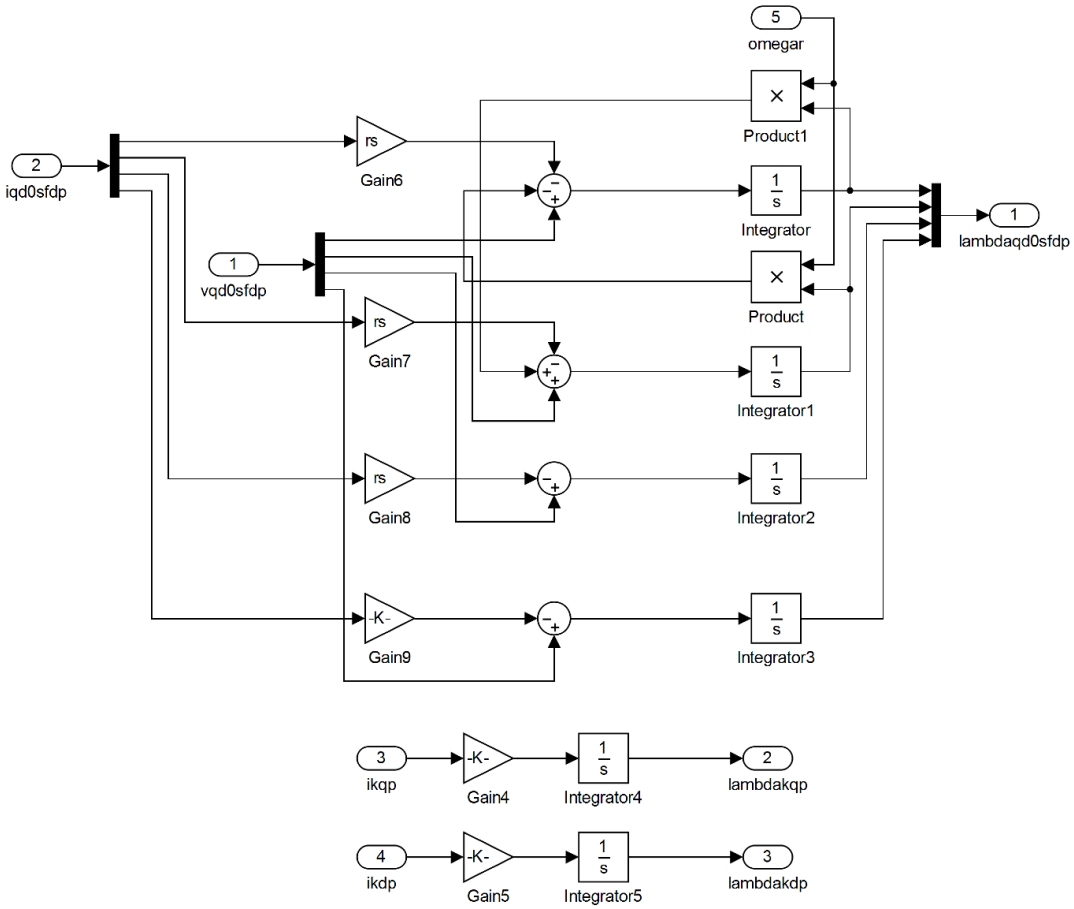

Figure 22. Flux Dynamics Sub-Model

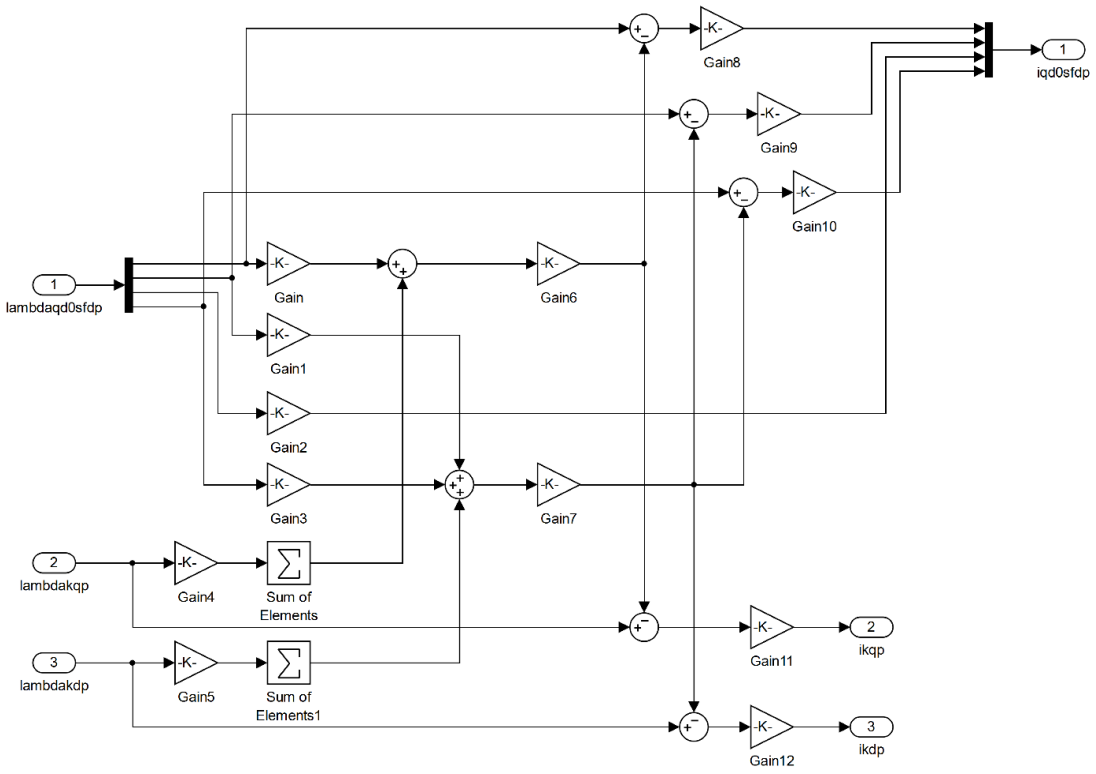

Figure 23. Currents Sub-Model

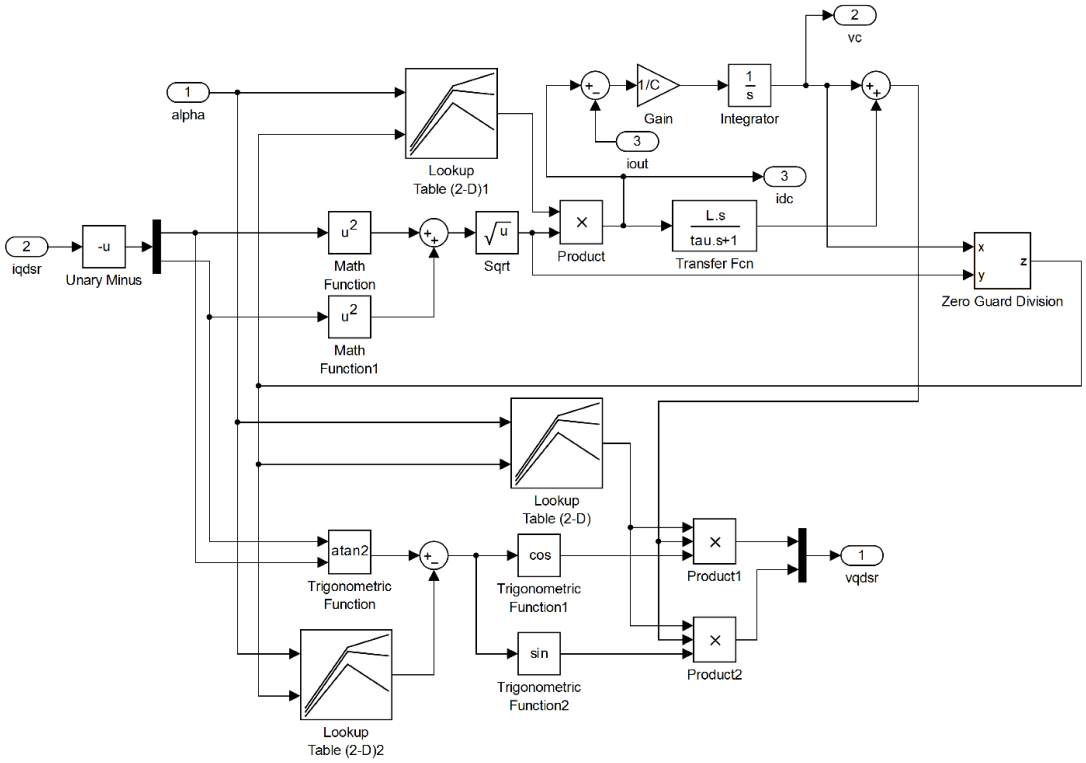

Figure 24. Rectifier Sub-Model

The Rectifier sub-model implements the core calculations of the AVM and determines the rectifier block outputs of *vdc* and *idc* based on lookup tables for the AVM parameters γ, β, and φ obtained from simulation using the detailed model.

7. STUDY OF PHYSICAL SYSTEM

Physical System Description

The physical system studied herein consists of a synchronous-generator/controlled-rectifier. The generator is a Marathon Electric 282PDL1705 three-phase, four-pole, 60 Hz synchronous generator which operates at 1800 rpm, controlled by an SE350 voltage regulator. It is coupled to a 15kW WEQ W22 induction motor regulated to operate at 1800 rpm by a Schneider Electric Altivar 71 Drive. The generator output is connected to a three-phase controlled rectifier and DC filter; the converter output is then connected to a configurable DC load bank.

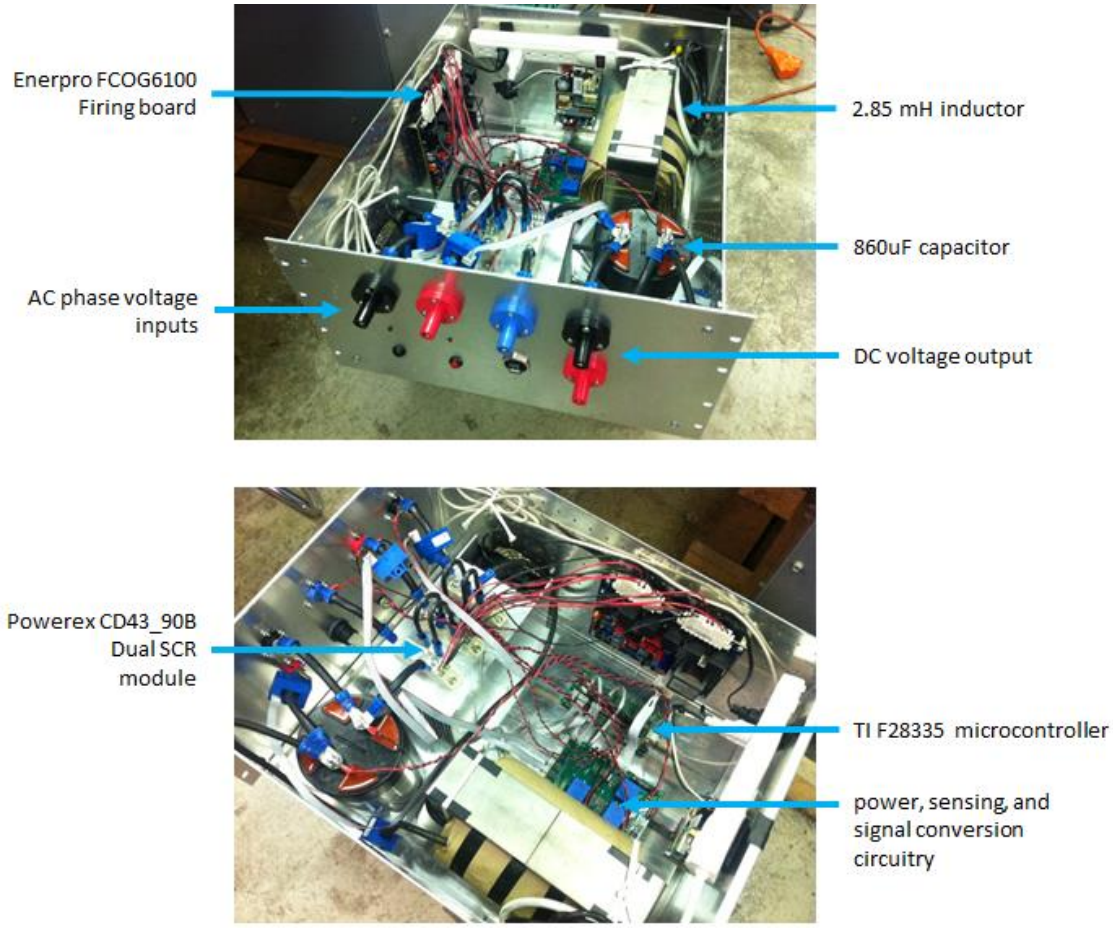

Figure 25. Controlled Rectifier Physical System

The converter consists of three Powerex CD43_90B Dual SCR modules connected in a full-bridge three-phase rectifier configuration, an output inductor with a design inductance of 2.85 mH, an 860 μF output capacitor (measured value of 848 μF), an Enerpro FCOG6100 firing board, a Texas Instruments microcontroller for control and monitoring, and auxiliary circuitry for power and signal routing and conversion.

Firing Angle Control

For thyristor firing control, the Enerpro board can provide a delay angle between roughly 10 and 140 degrees given an input voltage of 0 to 5 volts for the delay angle command signal (SIGHI). A PWM output from the microcontroller is output to an active low-pass filter to provide a 0-5V output corresponding to a 0-100% duty cycle PWM input. In order to exercise control of the delay angle via the microcontroller, it is desirable to relate the PWM duty cycle to the observed delay angle.

Since the load is passive and cannot supply power, under certain conditions the converter operates in discontinuous current mode (DCM). In this mode, during any intervals in which load current would be negative if the load could supply real power, the load current will be zero, since only positive current can flow through the resistive load. This discontinuity in the output current has an effect on the observed average voltage for a given delay angle.

A brief analysis of the converter was performed to estimate this effect. The three-phase rectifier output can be represented as the difference of two repeating voltages of period $\pi/6$ generated at the output by the switching sequence. One voltage, v_{top}, represents the positive-current intervals of the phase voltage inputs. To clarify, this corresponds to the voltage sources supplying positive current to the load during the firing of T1, T3, and T5. The other voltage,

v_{bottom}, represents the negative-current intervals, corresponding to the negative phase voltages during the firing of T2, T4, and T6. These voltages were described mathematically as follows:

$$v_{top} = \frac{\sqrt{2}V_{LL}}{\sqrt{3}}\cos\theta \qquad \theta \in \left[-\frac{\pi}{3}+\alpha, \frac{\pi}{3}+\alpha\right] \tag{90}$$

$$v_{bottom} = \frac{\sqrt{2}V_{LL}}{\sqrt{3}}\cos\left(\theta-\frac{\pi}{3}\right) \qquad \theta \in \left[\alpha, \frac{2\pi}{3}+\alpha\right] \tag{91}$$

The converter output voltage was expressed in terms of these voltages:

$$v = v_{top} - v_{bottom} \tag{92}$$

The average output voltage was then described as a signal consisting of a DC value and a first harmonic:

$$v = v_0 + V_1\cos(\omega t + \phi_{V1}) \tag{93}$$

The DC value and the coefficients of the first harmonic were calculated as follows:

$$v_0 = \frac{1}{2\pi}\int v\, d\theta \tag{94}$$

$$v_{a1} = \frac{1}{\pi}\int v\cos\theta\, d\theta \tag{95}$$

$$v_{b1} = \frac{1}{\pi}\int v\sin\theta\, d\theta \tag{96}$$

A phasor voltage for the first harmonic was then constructed from the coefficients:

$$\tilde{V}_1 = \sqrt{\frac{1}{2}({v_{a1}}^2 + {v_{b1}}^2)} \angle \tan^{-1}\left(\frac{v_{b1}}{v_{a1}}\right) \tag{97}$$

Using the DC and phasor voltage, and the known impedance of the output filter, a DC and phasor current were calculated:

$$i_0 = \frac{v_0}{R} \tag{98}$$

$$\tilde{I}_1 = \frac{\tilde{V}_1}{j\omega L + \frac{R/j\omega C}{R+1/j\omega C}} \tag{99}$$

The coefficients of the first-harmonic of the current were calculated

$$i_{a1} = \sqrt{2}\left|\tilde{I}_1\right| \cos\left(\angle \tilde{I}_1\right) \tag{100}$$

$$i_{b1} = \sqrt{2}\left|\tilde{I}_1\right| \sin\left(\angle \tilde{I}_1\right) \tag{101}$$

Knowing the DC and first-harmonic coefficients of the current, it can expressed as such:

$$i = i_0 + i_{a1} \cos\theta + i_{b1} \sin\theta \tag{102}$$

The analytical formulation of the current was then modified so that values for which $i < 0$ were set to 0, representing the operation of the converter in DCM. Using this model of the current, the average output current and load voltage are easily calculated.

$$\bar{\imath} = \frac{1}{2\pi} \int i \, d\theta \tag{103}$$

$$v_{out} = R\bar{\imath} \tag{104}$$

A preliminary study of system operation with three-phase 208V line-to-line input from a fixed source was completed to gather voltage output for an array of firing angle duty cycle commands. The data was then fit to the described model in order to determine an accurate relationship between the microcontroller duty cycle command and the firing angle α. The results are shown in **Figure 26**. The effect of DCM operation is illustrated in the data and the calculated relationship. For an ideal converter, the average output voltage is zero for $\alpha = \pi/2$ and becomes negative for $\alpha > \pi/2$. The measured output voltage does not reach zero even for low duty cycles corresponding to $\alpha > \pi/2$. Furthermore, the modified model of output voltage compensating for DCM provided an excellent fit to measured data.

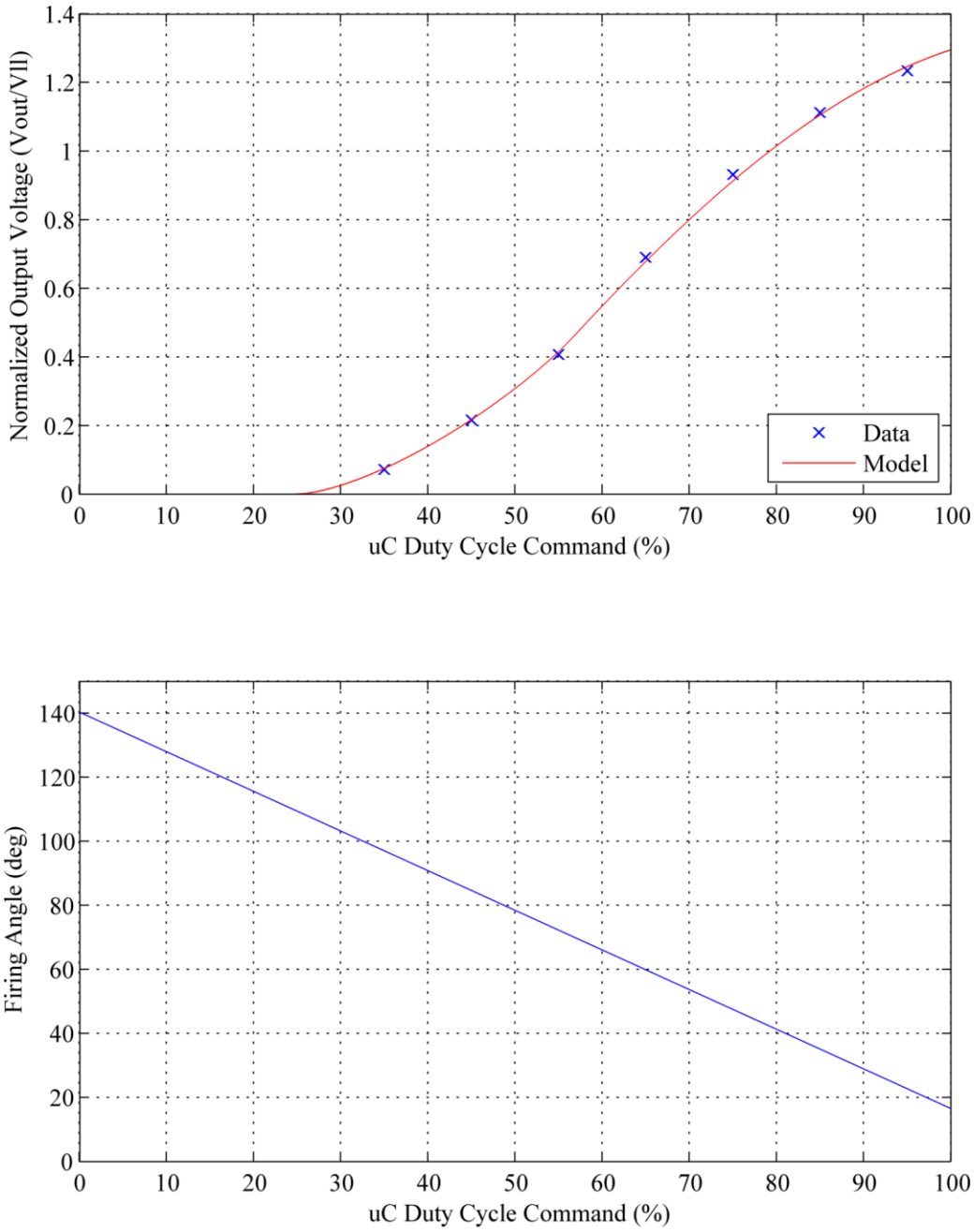

Figure 26. Duty Cycle Command vs. Firing Angle and Normalized Output Voltage

The relationship between the duty cycle and firing angle was ultimately defined through direct measurement of a diagnostic signal on the Enerpro firing board. Measuring this signal provides a pulse width which corresponds to the current delay angle. Repeating this measurement for several duty cycle values (0.05, 0.15, 0.25, 0.35, 0.45, 0.55, 0.65, 0.75, 0.85, 0.95) yielded the

following measurements and trend seen in the figure below. The fitted equation was used in the closed-loop control AVM simulation model as a basis for conversion from duty cycle to firing angle. It was also used to estimate alpha for the preliminary exciter fitting data as well as the step alpha changes as described below.

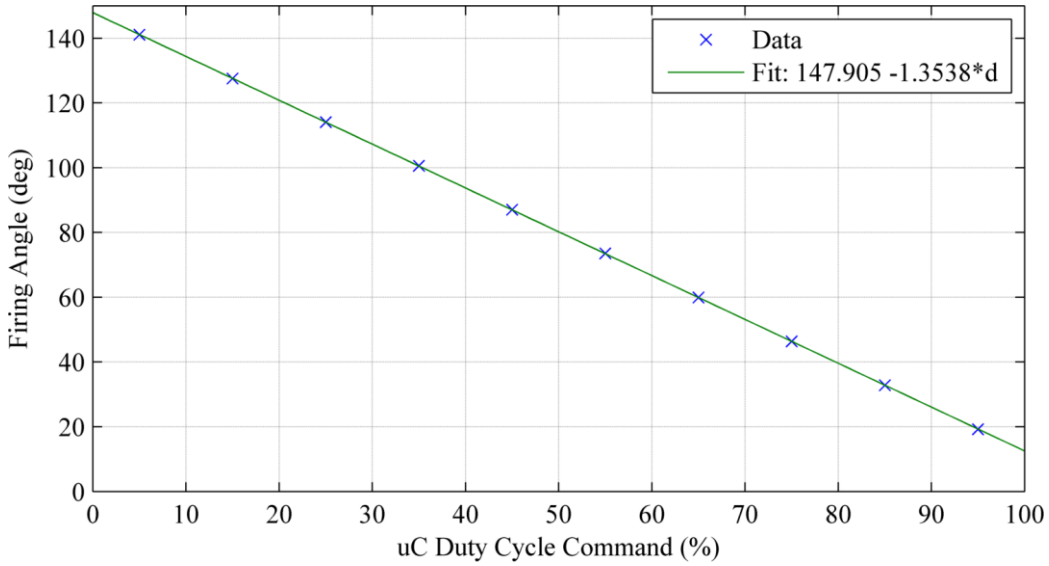

Figure 27. Duty Cycle Command vs. Firing Angle and Normalized Output Voltage

Preliminary Study and Fitting

An initial generator study was used to acquire data to tune AVM parameters to generator behavior. This study consisted of observing the DC output current and voltage of the converter before, during, and after a step load change from 20.5 Ω to 15.4 Ω, with a constant duty cycle command of 0.8913 (α = 27.07° as calculated by the duty cycle/alpha relationship in **Figure 27**). This provided initial data needed to fit the AVM parameters, specifically parameters of the excitation system, to best match the measured steady-state and dynamic data for the system.

A GA-based approach was used to determine the excitation system parameters. The excitation system model used was based primarily on elements of the AC1A and AC8B Excitation

System models in the IEEE Recommended Practices for Excitation System Models [18], with some non-essential elements omitted.

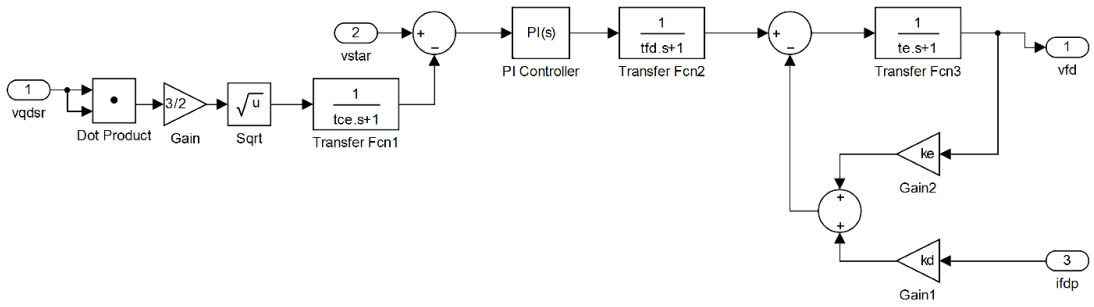

Figure 28. AVM Excitation System Model

The reference voltage, *vstar*, corresponds to the rms voltage output of the generator, chosen by the genetic algorithm from a range of 200-210V. The control consists of a PI controller element, several filter elements, and feedback paths for the field voltage and field current. The chosen exciter parameters are listed below.

Table 7. Fitted Exciter Parameters for AVM Exciter Model

tce	0.0010
vstar	204.7
kp	0.3262
ki	1.9217
te	0.01
kd	0.6383
tfd	2.930e-4
ke	1.283e-3

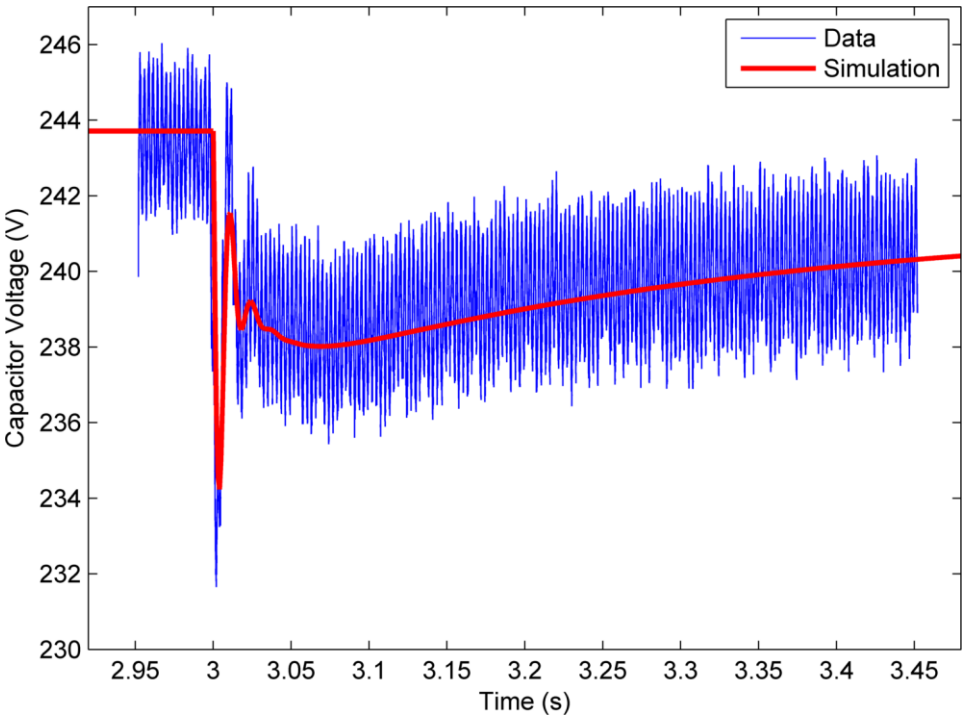

Figure 29. Capacitor Voltage for step load change, 20.5 Ω to 15.4 Ω, $\alpha \sim 27°$

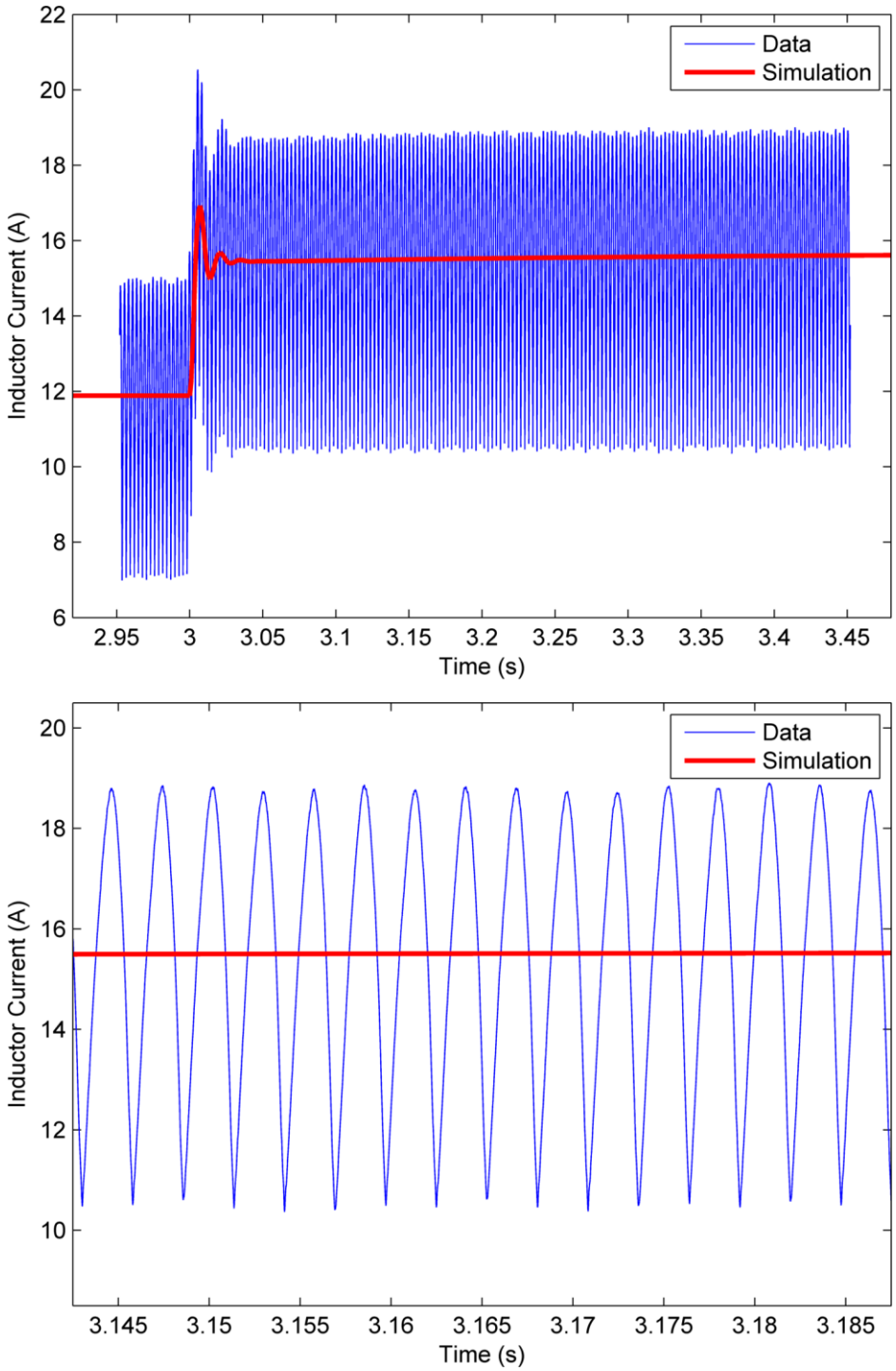

Figure 30. Inductor Current, full-scale and zoomed, for step load change, 20.5 Ω to 15.4 Ω, $\alpha \sim 27°$

The simulation output and measured data for the step load change are shown in **Figure 29** and **Figure 30.**

Generator Validation Studies

After the determination of the excitation system model and parameters, generator studies were performed to verify the AVM model behavior against measured data for an uncontrolled step load change, an uncontrolled step alpha change, and a step load change with software-implemented closed-loop control.

The step alpha change was implemented by toggling the duty-cycle command between 0.8701 and 0.6493 ($\alpha = 30°$ and $\alpha = 60°$ as calculated by the duty cycle/alpha relationship in **Figure 27**). Due to uncertainties in alpha as commanded by the firing board and the duty cycle/alpha relationship, the values for alpha in simulation required adjustment to provide an acceptable result ($\alpha = 29.2°$ and $\alpha = 61.8°$).

The closed-loop control consists of a software-implemented PI controller that regulates the converter output by controlling the delay angle. The parameters of the simulated PI control block (**Figure 31**), including *vcstar* = 220, *kp* = 0.001, *ki* = 0.05, and *tauf* = 4.42e-2, were duplicated in the software implementation. The following figures show the simulated and measured DC capacitor voltage and inductor current for the step load change, step alpha change, and step load change with PI control.

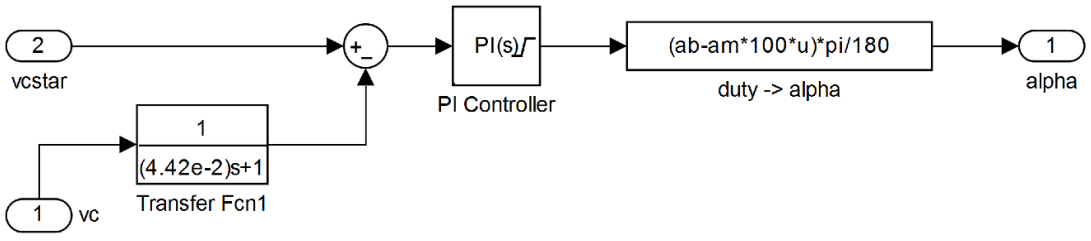

Figure 31. AVM PI Control Block

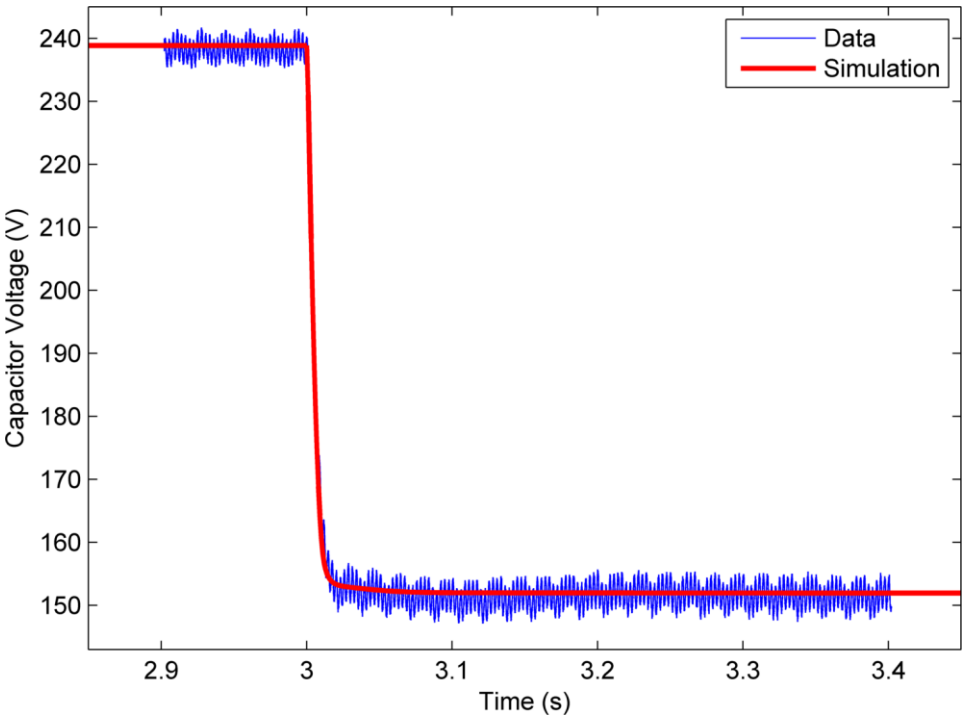

Figure 32. Capacitor Voltage for step alpha change, α = 29.2° to α = 61.8°

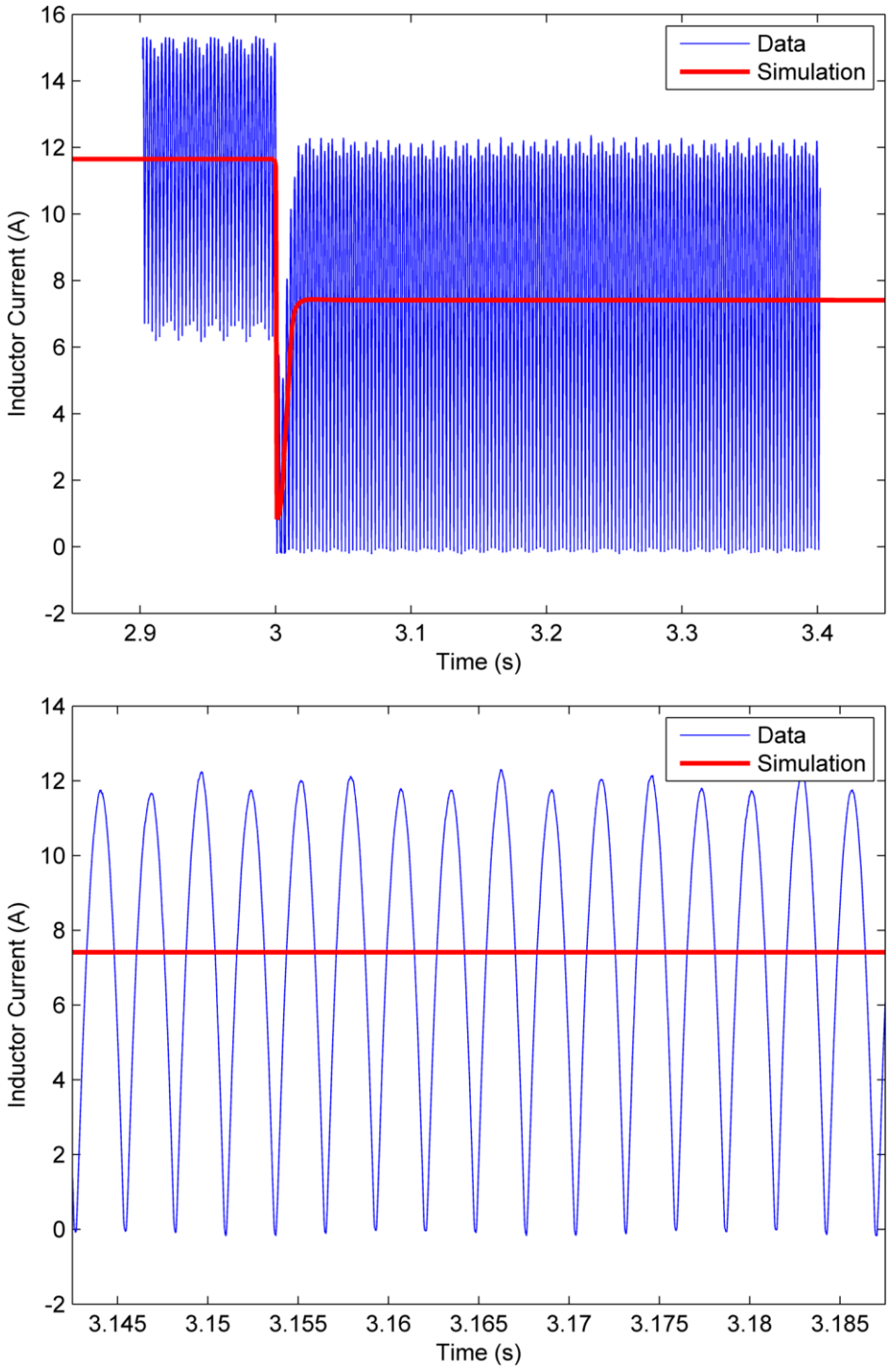

Figure 33. Inductor Current, full-scale and zoomed, for step alpha change, α = 29.2° to α = 61.8°

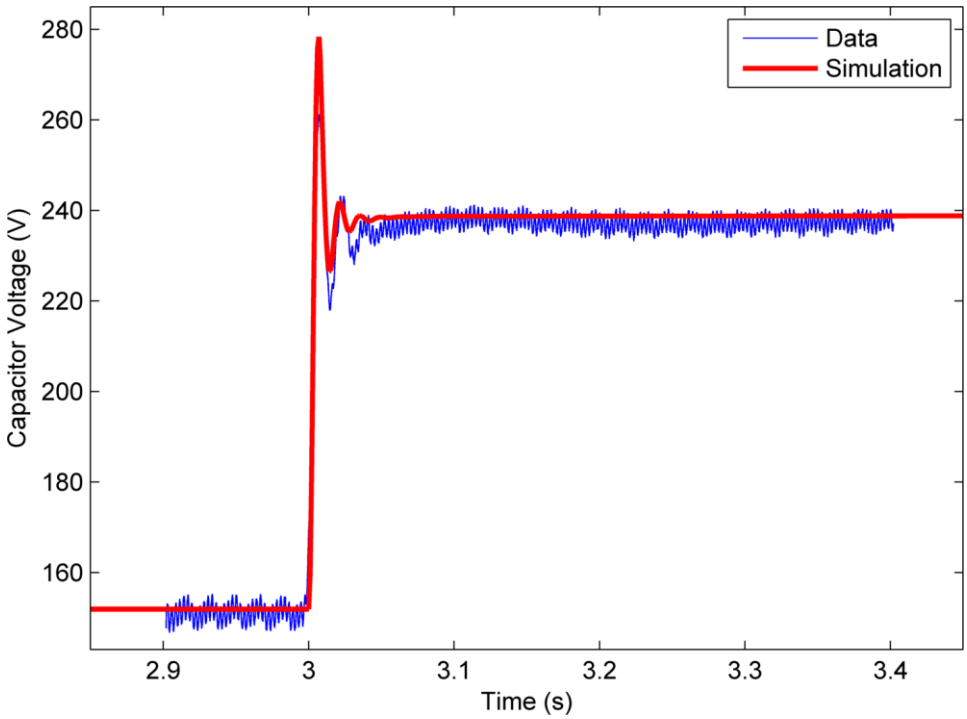

Figure 34. Capacitor Voltage for step alpha change, α = 61.8° to α = 29.2°

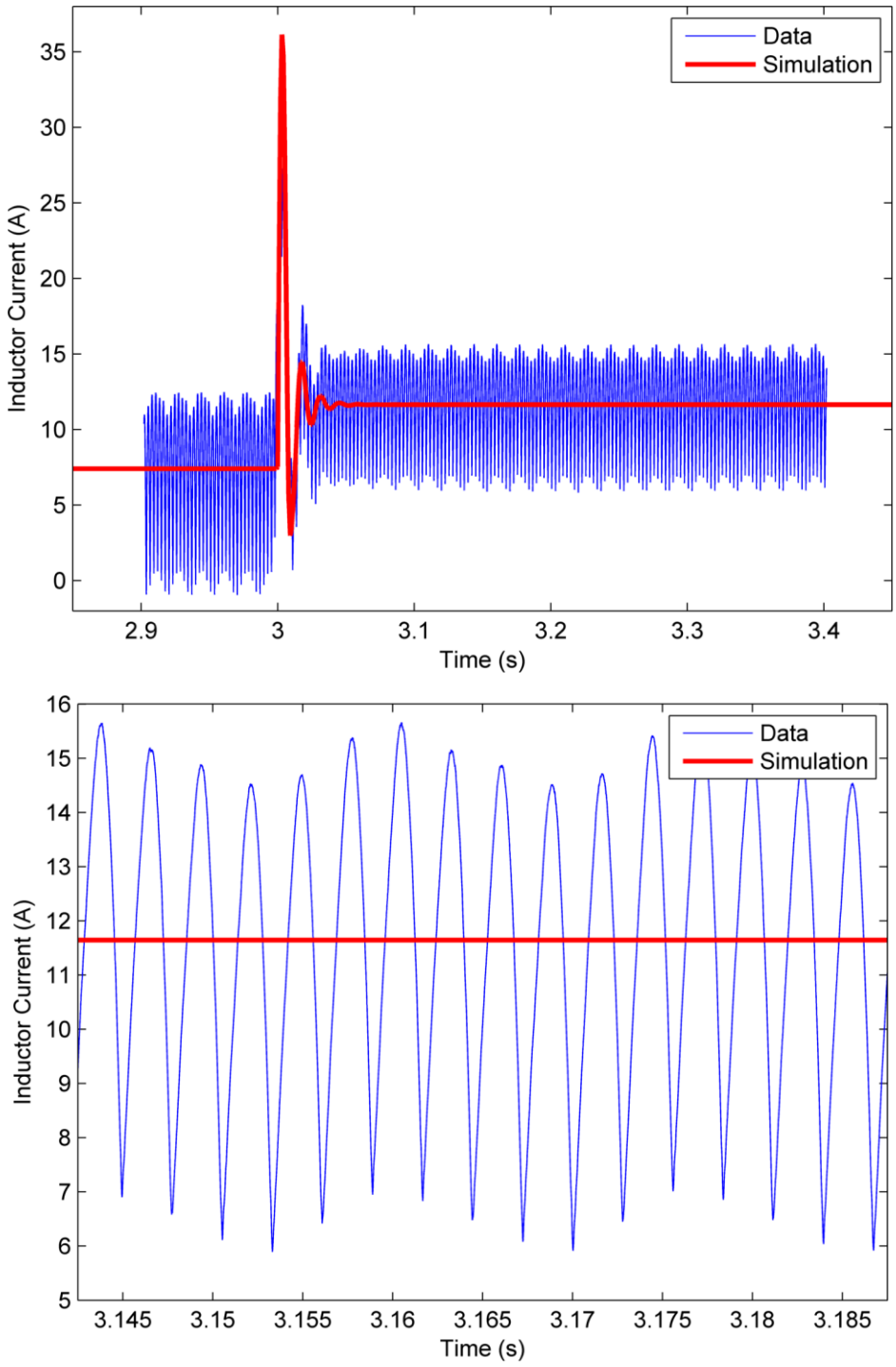

Figure 35. Inductor Current, full-scale and zoomed, for step alpha change, α = 61.8° to α = 29.2°

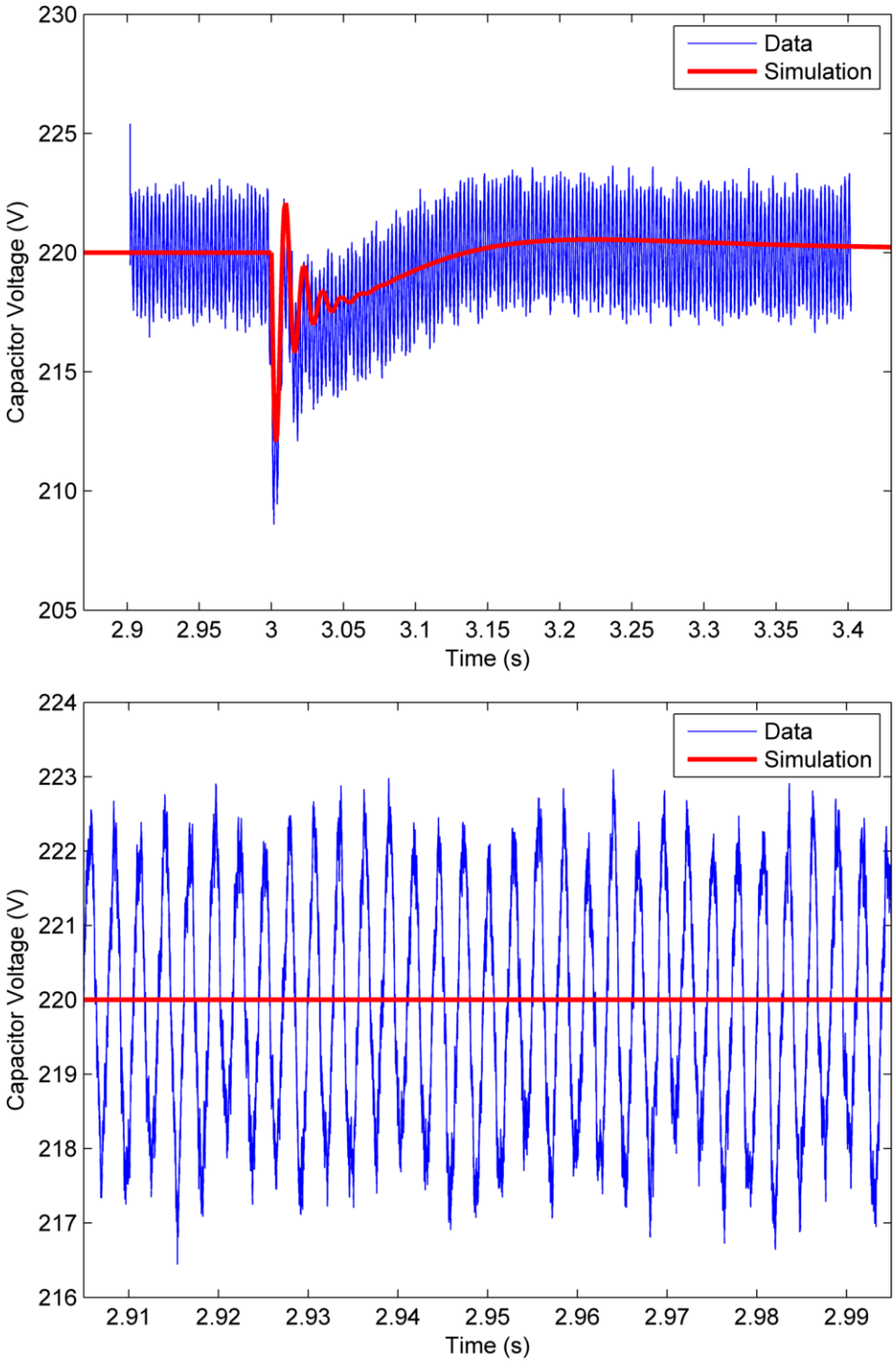

Figure 36. Capacitor Voltage, full-scale and zoomed, for closed-loop control with step load change, 20.5 Ω to 15.4 Ω

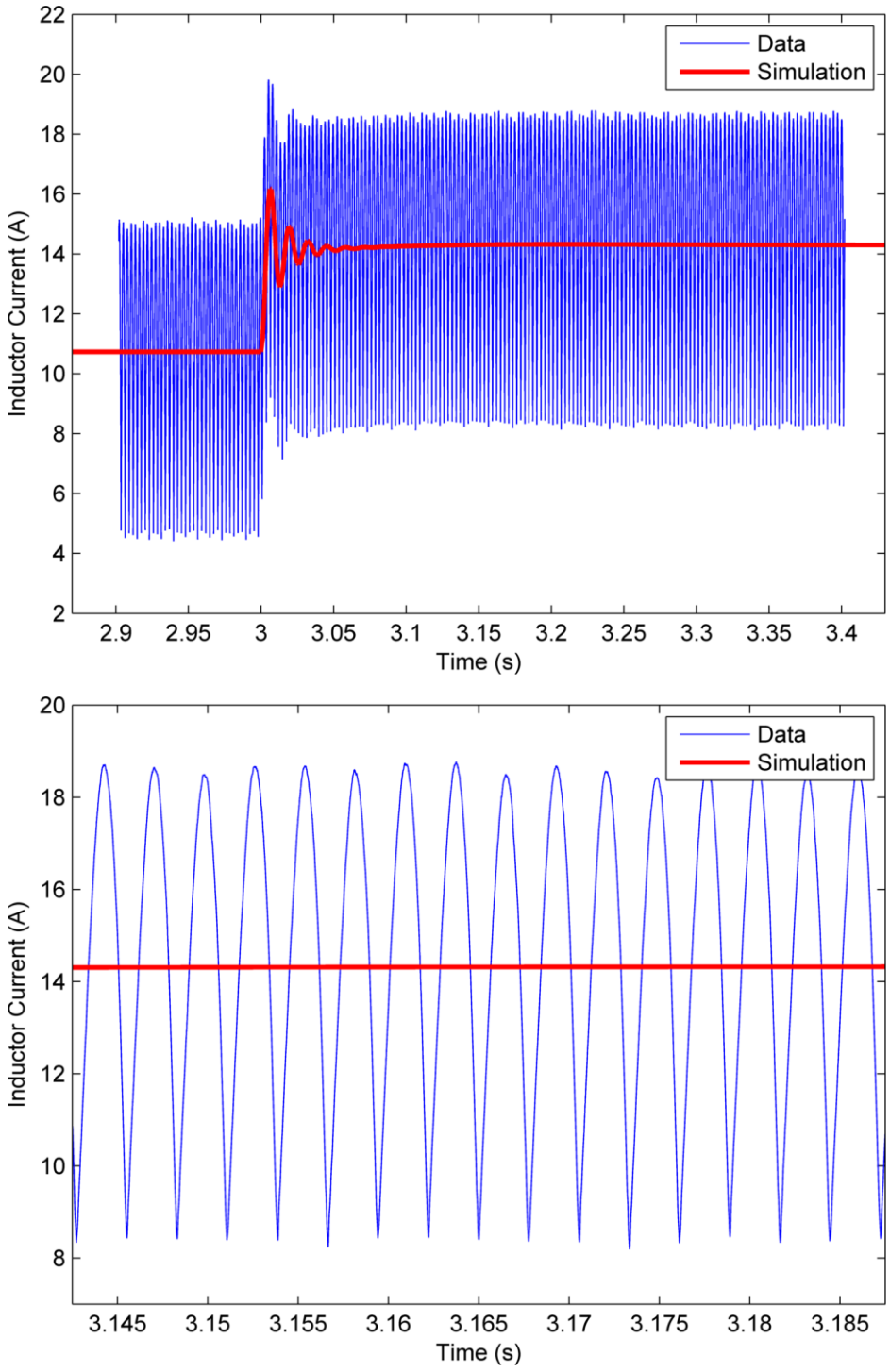

Figure 37. Inductor Current, full-scale and zoomed, for closed-loop control with step load change, 20.5 Ω to 15.4 Ω

8. CONCLUSION

In summary, the hardware validation of a novel average value model simulation for a synchronous-generator/controlled-rectifier system was presented. It is concluded that the AVM method used herein provides an acceptable model of the system for predicting transient and steady-state performance for a variety of loading and operating conditions including step load changes, changes in delay angle, and external closed-loop control. Using Standstill Frequency Response techniques to characterize the generator for hardware validation proved to be a relatively simple, versatile, and accurate method, providing the necessary information to represent the generator in both the detailed model and the average-value model. An adequate fit to the SSFR data was found using genetic algorithm techniques to search a large solution space and arrive at a set of parameters. The modeling and fitting of the generator excitation was somewhat difficult, requiring multiple trials and approaches before devising a model that yielded an acceptable fit for the dynamic and steady-state behavior of the system.

Possible improvements for future research would include a more accurate characterization of the machine studied herein (Marathon Electric 282PDL1705) and further experimental validation of the overall model, as well as investigation of the model validity when used within system-level studies. The generator characterization obtained via SSFR measurement procedures and analysis by genetic algorithm may be improved by modeling the *q* and *d*-axis generator equivalent circuits as arbitrary networks, allowing for greater precision and uniqueness of the derived parameters. In addition, further experimentation with the exciter model could yield favorable results, but the current configuration provides sufficient validation for the model.

REFERENCES

[1] I. Report, "Proposed Excitation System Definitions for Synchronous Machines," *Power Apparatus and Systems, IEEE Transactions on,* Vols. PAS-88, no. 8, pp. 1248-1258, Aug 1969.

[2] T. Jahns and M. Maldonado, "A new resonant link aircraft power generating system," *Aerospace and Electronic Systems, IEEE Transactions on,* vol. 29, no. 1, pp. 206-214, Jan 1993.

[3] J. Jatskevich, S. Pekarek and A. Davoudi, "Parametric average-value model of synchronous machine-rectifier systems," *Energy Conversion, IEEE Transactions on,* vol. 21, no. 1, pp. 9-18, March 2006.

[4] P. W. O. S. S. Krause, Analysis of Electric Machinery and Drive Systems, Wiley-IEEE Press, 2002.

[5] S. Crary, "Two-reaction theory of synchronous machines," *Electrical Engineering,* vol. 56, no. 1, pp. 27-31, Jan 1937.

[6] P. Krein, Elements of Power Electronics, Oxford University Press, 1997.

[7] P. Pejović and J. Kolar, "An analysis of three-phase rectifiers with constant voltage loads," in *Circuits and Systems for Communications (ECCSC), 2010 5th European Conference on*, 2010.

[8] H. Petroson and P. Krause, "A Direct-and Quadrature-Axis Representation of a Parallel AC and DC Power System," *Power Apparatus and Systems, IEEE Transactions on,* Vols. PAS-85, no. 3, pp. 210-225, March 1966.

[9] M. Demiroglu and J. Mayer, "Steady-state characteristics of synchronous machine-line-commutated converter systems," *Energy Conversion, IEEE Transactions on,* vol. 17, no. 2, pp. 234-241, Jun 2002.

[10] H. Atighechi, S. Chiniforoosh and J. Jatskevich, "Approximate dynamic average-value model for controlled line-commuted converters," in *Electrical and Computer Engineering (CCECE), 2011 24th Canadian Conference on*, 2011.

[11] J. T. Alt, S. Sudhoff and B. E. Ladd, "Analysis and average-value modeling of an inductorless synchronous machine load commutated converter system," *Energy Conversion, IEEE Transactions on,* vol. 14, no. 1, pp. 37-43, Mar 1999.

[12] S. Sudhoff, K. A. Corzine, H. Hegner and D. Delisle, "Transient and dynamic average-value modeling of synchronous machine fed load-commutated converters," *Energy Conversion, IEEE Transactions on,* vol. 11, no. 3, pp. 508-514, Sep 1996.

[13] D. Aliprantis, S. Sudhoff and B. Kuhn, "A brushless exciter model incorporating multiple rectifier modes and Preisach's hysteresis theory," *Energy Conversion, IEEE Transactions on,* vol. 21, no. 1, pp. 136-147, March 2006.

[14] J. Jatskevich, S. Pekarek and A. Davoudi, "A fast procedure for constructing an accurate dynamic average-value model of synchronous machine-rectifier systems," in *Power Engineering Society General Meeting, 2006. IEEE*, 2006.

[15] Y. Li, "Numerical Averaging of a Synchronous-Machine/Controlled-Rectifier System," Lexington, KY, 2012.

[16] "IEEE Guide for Test Procedures for Synchronous Machines Part IAcceptance and Performance Testing Part IITest Procedures and Parameter Determination for Dynamic Analysis," *IEEE Std 115-2009 (Revision of IEEE Std 115-1995),* pp. 1-219, May 2010.

[17] "IEEE Standard Procedures for Obtaining Synchronous Machine Parameters by Standstill Frequency Response Testing (Supplement to ANSI/IEEE Std 115-1983, IEEE Guide: Test Procedures for Synchronous Machines)," *IEEE Std 115A-1987,* pp. 0_1-, 1987.

[18] "IEEE Recommended Practice for Excitation System Models for Power System Stability Studies," *IEEE Std 421.5-2005 (Revision of IEEE Std 421.5-1992),* pp. 0_1-85, 2006.

[19] J. Kettleborough, I. Smith and B. A. Fanthome, "Simulation of a dedicated aircraft generator supplying a heavy rectified load," *Electric Power Applications, IEE Proceedings B,* vol. 130, no. 6, pp. 431-435, November 1983.

[20] D. Aliprantis, S. Sudhoff and B. Kuhn, "Genetic algorithm-based parameter identification of a hysteretic brushless exciter model," *Energy Conversion, IEEE Transactions on,* vol. 21, no. 1, pp. 148-154, March 2006.

[21] D. Aliprantis, S. Sudhoff and B. Kuhn, "Experimental Characterization Procedure for a Synchronous Machine Model With Saturation and Arbitrary Rotor Network Representation," *Energy Conversion, IEEE Transactions on,* vol. 20, no. 3, pp. 595-603, Sept 2005.

[22] S. Sudhoff and O. Wasynczuk, "Analysis and average-value modeling of line-commutated converter-synchronous machine systems," *Energy Conversion, IEEE Transactions on,* vol. 8, no. 1, pp. 92-99, Mar 1993.

[23] S. Sudhoff, "Analysis and average-value modeling of dual line-commutated converter-6-phase synchronous machine systems," *Energy Conversion, IEEE Transactions on,* vol. 8, no. 3, pp. 411-417, Sep 1993.

[24] S. D. Sudhoff, D. C. Aliprantis, B. T. Kuhn and P. L. Chapman, "Experimental Characterization Procedure for Use with an Advanced Induction Machine Model," *Power Engineering Review, IEEE,* vol. 22, no. 12, pp. 57-57, Dec 2002.

[25] C.-M. Ong, Dynamic Simulation of Electric Machinery, Prentice-Hall, 1997.

VITA

Kyle Hord was born in Louisville, KY. He received his Bachelor's Degree in Electrical Engineering from the University of Kentucky, Lexington, KY in May 2009. In September 2010 he enrolled as a MSEE student at the University of Kentucky under scholarship as part of the Power and Energy Institute of Kentucky (PEIK) program.